Journal of Molecular Structure 1244 (2021) 130947

Contents lists available at ScienceDirect

Journal of Molecular Structure

journal homepage: www.elsevier.com/locate/molstr

# Synthesis, Characterization, Crystal Structure, Hirshfeld surface analysis and DFT studies of novel compounds based on the methoxynaphthalene ring

El-Mahdi Ourhzif[a,b,c], Isabelle Abrunhosa-Thomas[a], Pierre Chalard[a], Mostafa Khouili[c], Yves Troin[a], Mohamed Akssira[b,*], El Mostafa Ketatni[c,*]

[a] Université Clermont Auvergne, CNRS, SIGMA Clermont, ICCF, F-63000 Clermont-Ferrand, France
[b] Laboratoire de Chimie Physique et Chimie Bioorganique, URAC 22 Université Hassan II, Casablanca, FST, BP 146, 28800, Mohammedia, Morocco
[c] Laboratory of Organic and Analytical Chemistry, Sultan Moulay Slimane University, Faculty of Science and Technology, BP 523, 23000 Beni-Mellal, Morocco

ARTICLE INFO

*Article history:*
Received 16 May 2021
Revised 14 June 2021
Accepted 17 June 2021
Available online 22 June 2021

*Keywords:*
Methoxynaphthalene
Crystal Structure
Hydrogen bond
C—H...$\pi$ interactions
Hirshfeld surface analysis
Density Functional Theory

ABSTRACT

Polysubstituted naphthalenes and their analogues have been found in nature or synthesized, and have attracted increasing attention due to their numerous pharmacological and biological activities. The present study describes a synthesis of novel series of methoxynaphthalene derivatives using the Stobbe condensation reaction method. The chemical structures of these compounds were confirmed by spectroscopic techniques such as $^{1}$H and $^{13}$C NMR, IR, LC-HRMS spectral data and X-ray crystallography. The supramolecular assembly in the structures reported here is dominated by C—H···O hydrogen bonds for compounds **5, 6, 8, 11, 14** and **17** and O—H···O for compound **12**. The molecules are also arranged by C–H···$\pi$ interaction and/or $\pi-\pi$ stacking, which are responsible for the formation and stability of the molecular assemblies. Hirshfeld surface analysis was also performed in order to obtain reliable structural information in concurrence with experimental results, and intermolecular interactions that exist inside the crystal have been investigated. Additionally, DFT calculations have been used to analyze the electronic and geometric frontier molecular orbital and Molecular Electrostatic Potential map analyses of the compounds were produced using the optimized structures.



## 1. Introduction

The present investigation is a continuation of our broad programme work on the synthesis and structural study of methoxynaphthalenes and its derivatives and to understand the geometrical features and the underlying intermolecular interactions. Substituted naphthalenes are important constituents of many natural products, pharmaceuticals and bioactive compounds [1-5], which have two aromatic rings (A-ring and B-ring), such as marmelin [6], parvinaphthol B [7], lawsonaphthoate A [8], guieranone A [9], furomollugin [10] and justicidine A [11] (Fig. 1). They are abundant in plants where they are considered to be the precursors of biaryl ring systems and arylnaphthalene lignans [12-15]. A number of substituted naphthalenes have attracted much attention owing to their pharmaceutical and biological importance, which constitute an important group of natural and synthetic products that have been screened for a wide range of pharmacological activities such as anti-inflammatory, [8,12,16] antitumor [6-7,17-18], antiviral [10,19], antidiabetic [20], antiplatelet [11,21], anti-HIV [22], and antimalarial properties [23] (Fig. 1). The biological applications of this class of compounds were recently reviewed [24].

More particularly, a number of synthetic and natural methoxynaphthalenes exhibited potent anticancer activity against many cancer cell lines. Even simple compounds for example Guieranone A showed considerable anticancer properties. [25] Moreover, substituted naphthalene-based compounds offer a high degree of structural diversity and have proven to be broadly useful as therapeutics [24]. The naphthalene moiety is the core structure in many drugs such as Naphyrone, Nafimidone, Naftifine, Propranolol, Duloxetine and Nabumetone (Fig. 2) [24]. Additionally, this structural motif is a primary scaffold in numerous applications in supramolecular chemistry and material science because of their unique photochemical, photoconductivity, and electroluminescent properties [26-30].

The development of new methoxynaphthalene-based structures requires a great deal of effort in synthesis methodology

* Corresponding authors.
*E-mail addresses:* akssira.m@gmail.com (M. Akssira), elm_ketatni@hotmail.fr (E.M. Ketatni).

https://doi.org/10.1016/j.molstruc.2021.130947
0022-2860/

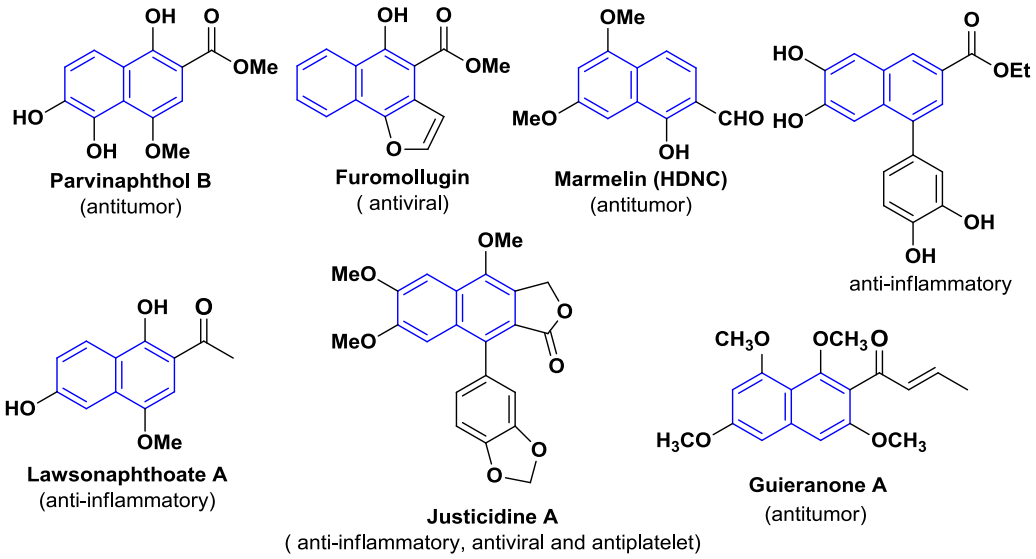


**Fig. 1.** Examples of natural products derived from substituted naphthalenes.

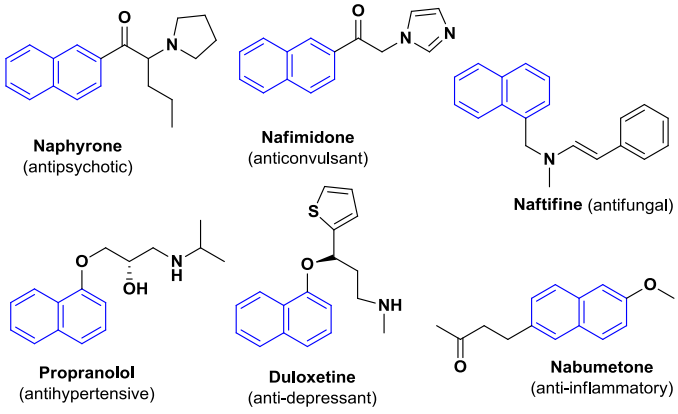


**Fig. 2.** Some drugs containing the naphthalene moiety.

and architectural design. Several methods for synthesizing methoxynaphthalenes and derivates have been described by the scientific community [31-34], and the most typical reaction involves the Stobbe condensation method. This method consists in a reaction between an aromatic aldehyde with a diethyl or dimethyl succinate [35-37]. In this work, we report the synthesis and characterization of a novel series of substituted naphthathalene derivatives and, recently, we reported the structure of the following three naphthalene derivatives ethyl 4-acetoxy-3-bromo-6,7-dimethoxy-2-naphthoate (**8**) (CCDC: 2050380), 6,7-dimethoxy-9-methyl-1-oxo-1,3-dihydronaphtho[2,3-c]furan-4-yl trifluoromethanesulfonate (**14**) (CCDC: 2050379) and ethyl 1-cyano-6,7-dimethoxy-4-((trifluoromethylsulfonyl)oxy)-2-naphthoate (**17**) (CCDC: 2050387) [38], which were prepared from ethyl 4-hydroxy-6,7-dimethoxy-2-naphthoate (**1**) using the Stobbe condensation reaction method from 3,4-dimethoxy benzaldehyde with diethyl succinate [39].

The newly synthesized compounds were characterized using elemental analysis, $^{1}H$ and $^{13}C$ NMR, IR and LC-HRMS techniques, except the compounds **7, 8** and **13-17:** the synthesis of the latter is described recently [38]. Further, crystal structures were confirmed using X-ray diffraction method. Quantum chemical calculations were carried out using density functional theory (DFT) to analyze the electronic and geometric frontier molecular orbital and molecular electrostatic potential (MEP) map analyses of the compounds were produced using the optimized structures.

## 2. Experimental section

### 2.1. Chemicals and instrumentation

Starting materials were obtained from commercial suppliers and used without further purification. **IR** spectra were obtained using an IRAffinity-1S FTIR Infrared spectrophotometer. Measurements were made by loading the sample directly onto a diamond cell. The measurements are reported on the wavenumber scale ($cm^{-1}$). **NMR** spectra, performed on a Bruker Avance 400 ($^{1}H$: 400 MHz, $^{13}C$: 100 MHz), are reported in ppm using the solvent residual peak as an internal standard. High resolution mass spectra (**HRMS**) (ESI+) were determined on a high-resolution Waters Micro Q-ToF apparatus. **LC–MS** was recorded on a Q Exactive Quadrupole-Orbitrap mass spectrometer coupled to a HPLC Ultimate 3000 (Kinetex EVO C18; 1.7 $\mu$m; 100 mm $\times$ 2.1 mm column with a flow rate of 0.45 mL $min^{-1}$ with the following gradient: a linear gradient of solvent B from 5% to 95% over 7.5 min (solvent A = $H_2O$ + 0.1% formic acid, solvent B = acetonitrile + 0.1% formic acid) equipped with a DAD UV/vis 3000 RS detector (UCA-Partner, Université Clermont Auvergne, Clermont-Ferrand, France). Chromatographic purifications were performed by column chromatography using 40–63 $\mu$m silica gel. Reactions were monitored by TLC using fluorescent silica gel plates (60 F254 from Merck). Melting points **(mp)** were measured on a Kofler hot bench or Reichert plate-heating microscope and are reported uncorrected.

#### 2.1.1. Synthesis of ethyl 4,6,7-trimethoxy-2-naphthoate (2)

To a solution of ethyl 4-hydroxy-6,7-dimethoxy-2-naphthoate **1** [39] (3.0 g, 10.86 mmol) in acetone (100 mL) were added successively potassium carbonate (1.50 g, 10.86 mmol) and dimethyl sulphate (2.06 mL, 21.72 mmol). The mixture was refluxed at room temperature for 12 h, the insoluble fraction was filtered off, and the filtrate was concentrated *in vacuo*. The residue was dissolved in $CH_2Cl_2$ (50 mL), then the $CH_2Cl_2$ solution was washed with aqueous $NH_3$ (25%, 3 $\times$ 20 mL) and NaOH solution (5%, 50 mL), dried over $MgSO_4$, and concentrated in vacuo. Chromatography on silica gel (10% EtOAc /hexane) gave ethyl 4,6,7-trimethoxy-2-naphthoate **2** (3.0 g, 95% yield) as a white solid. $R_f$ = 0. 68 (30% EtOAc/hexane) mp: 112-113°C.

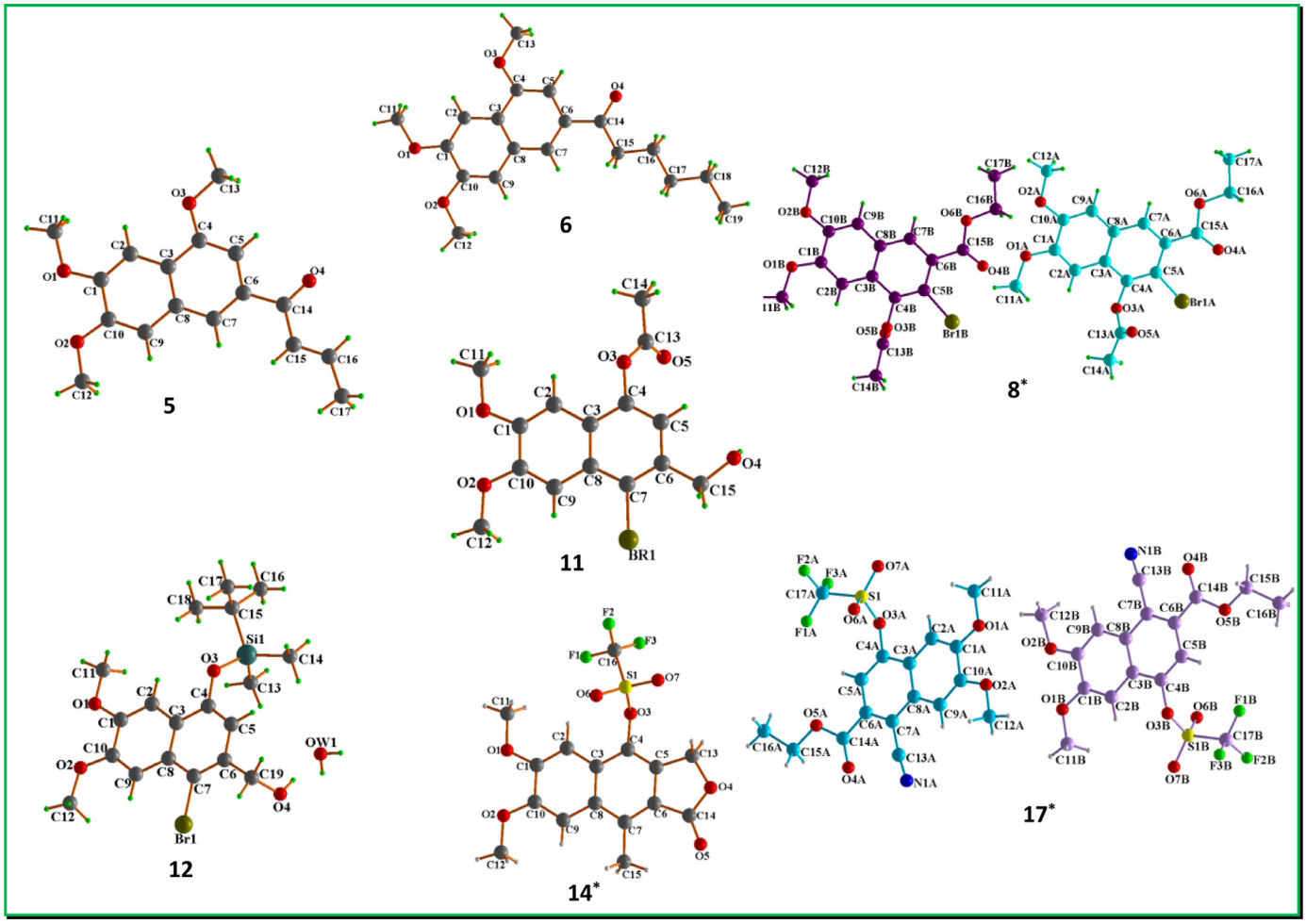


**Fig. 3.** The structures of **5, 6, 8, 11, 12, 14** and **17** showing the atom numbering with ellipsoids drawn at the 50% probability level. * ref [38].

IR $\nu_{max}$ ($cm^{-1}$): 1707, 1587, 1431, 1229, 1217, 1161, 1011,764. $^1H$ NMR (400 MHz, $CDCl_3$, $\delta$ ppm, $J$ Hz) $\delta$: = 1.42 (t, $J$ = 7.1 Hz, 3H), 3.98 (s, 3H), 4.02 (s, 3H), 4.03 (s, 3H), 4.41 (q, $J$ = 7.1Hz, 2H), 7.15 (s, 1H), 7.30 (s, 1H), 7.50 (s, 1H), 8.06 (s, 1H). $^{13}C$ NMR (100 MHz, $CDCl_3$) $\delta$: 167.2, 154.4, 150.8, 150.2, 129.2, 126.3, 123.4, 122.2, 107.4, 102.1, 101.1, 61.0, 56.0, 55.9, 55.7, 14.5. HRMS (ESI): *m/z* calcd for $C_{16}H_{19}O_5$ $[M+H]^+$ 291.1227; found 291.1231.

### 2.1.2. Synthesis of diethyl (2-oxo-2-(1,4,6,7-tetramethoxynaphthalen-2-yl)ethyl) phosphonate (3)

Butyl lithium solution in hexanes (2.5 M, 16.5 mL, 41.33 mmol) was added dropwise to a stirred solution of diethyl methylphosphonate (4.37 mL, 40.37 mmol) in THF (50 mL) under a nitrogen atmosphere at -78°C. The solution was stirred for 10 min at -78°C. Then, a solution of ester **2** in THF (10 mL) was added dropwise and stirred for 2 h at -78°C, and for 12 h at room temperature. The mixture was poured into ice and a 2 M HCl aqueous solution. The mixture was extracted with EtOAc. The organic layer was washed with water and brine and dried over anhydrous $MgSO_4$. The solvent was evaporated *in vacuo* and the residue was chromatographed on silica gel (90% EtOAc /hexane) to produce phosphonate **3** (1.28 g, 98% yield) as a green oil. $R_f$ = 0.27 (100% EtOAc).

IR $\nu_{max}$ ($cm^{-1}$): 1661, 1601, 1510, 1481, 1429, 1366, 1337, 1256, 1110, 1167, 1020, 1007, 960, 793. $^1H$ NMR (400 MHz, $CDCl_3$, $\delta$ ppm, $J$ Hz): $\delta$ = 7.96 (s, 1H), 7.43 (s, 1H), 7.25 (s, 1H), 7.12 (s, 1H), 4.08 (qu, $J$ = 7.1 Hz, 4H), 3.96 (s, 6H), 3.92 (s, 3H), 3.68 (s, 1H), 3.62 (s, 1H), 1.21 (t, $J$ = 7.1 Hz, 6H). $^{13}C$ NMR (100 MHz, $CDCl_3$): $\delta$ = 191.4, 154.6, 151.3, 150.2, 132.8, 128.9, 124.0, 123.6, 107.8, 101.0, 100.2, 62.5, 56.0, 55.8, 55.6, 38.0 ($J$ = 131 Hz), 16.2, 16.3. HRMS (ESI): *m/z* calcd for $C_{19}H_{25}O_7P$ $[M+H]^+$ 397.1411; found 397.1403.

### 2.1.3. Synthesis of N,4,6,7-tetramethoxy-N-methyl-2-naphthamide (4)

Compound **2** (1.0 g, 3.44 mmol) was dissolved in 5% KOH/MeOH: $H_2O$ (19:1) (100 mL) at 60°C, and the mixture was stirred at room temperature for 3 h. The reaction was quenched with aqueous citric acid and extracted with AcOEt. The organic layer was washed with brine, dried over $MgSO_4$, and evaporated. The residue was purified by column chromatography to afford 4,6,7-trimethoxy-2-naphthoic acid (0.860 g, 95% yield) as a white powder.

A solution of acid (0.800 g, 3.5 mmol), 1,1′-carbonyldiimidazole (0.660 g, 3.66 mmol) and methoxy(methyl)amine hydrochloride (0.893 g, 9.15 mmol) in dry $CH_2Cl_2$ (50 mL) was stirred at room temperature for 24 h. The mixture was washed with water (20 mL) and brine (20 mL), and the combined aqueous phases were extracted with $CH_2Cl_2$ (2 × 30 mL). The combined organic layers were dried over $MgSO_4$, filtered, concentrated *in vacuo* and purified by column chromatography to afford the title compound **4** as a white solid (0.645 g, 69%. $R_f$ = 0.33 (50% EtOAc/hexane); mp: 118-119°C.

IR $\nu_{max}$ ($cm^{-1}$): 1614, 1580, 1514, 1485, 1396, 1367, 1258, 1217, 1165, 1015, 841, 741. $^1H$ NMR (400 MHz, Acetone-$d_6$, $\delta$ ppm, $J$ Hz): $\delta$ = 7.71 (s, 1H), 7.51 (s, 1H), 7032 (s, 1H), 7.05 (s, 1H), 4.03 (s, 3H), 3.94 (s, 3H), 3.92 (s, 3H), 3.64 (s, 3H), 3.33 (s, 3H). $^{13}C$ NMR (100 MHz, Acetone-$d_6$, $\delta$ ppm, $J$ Hz): $\delta$ = 170.7, 154.8, 151.5, 151.4, 131.3,

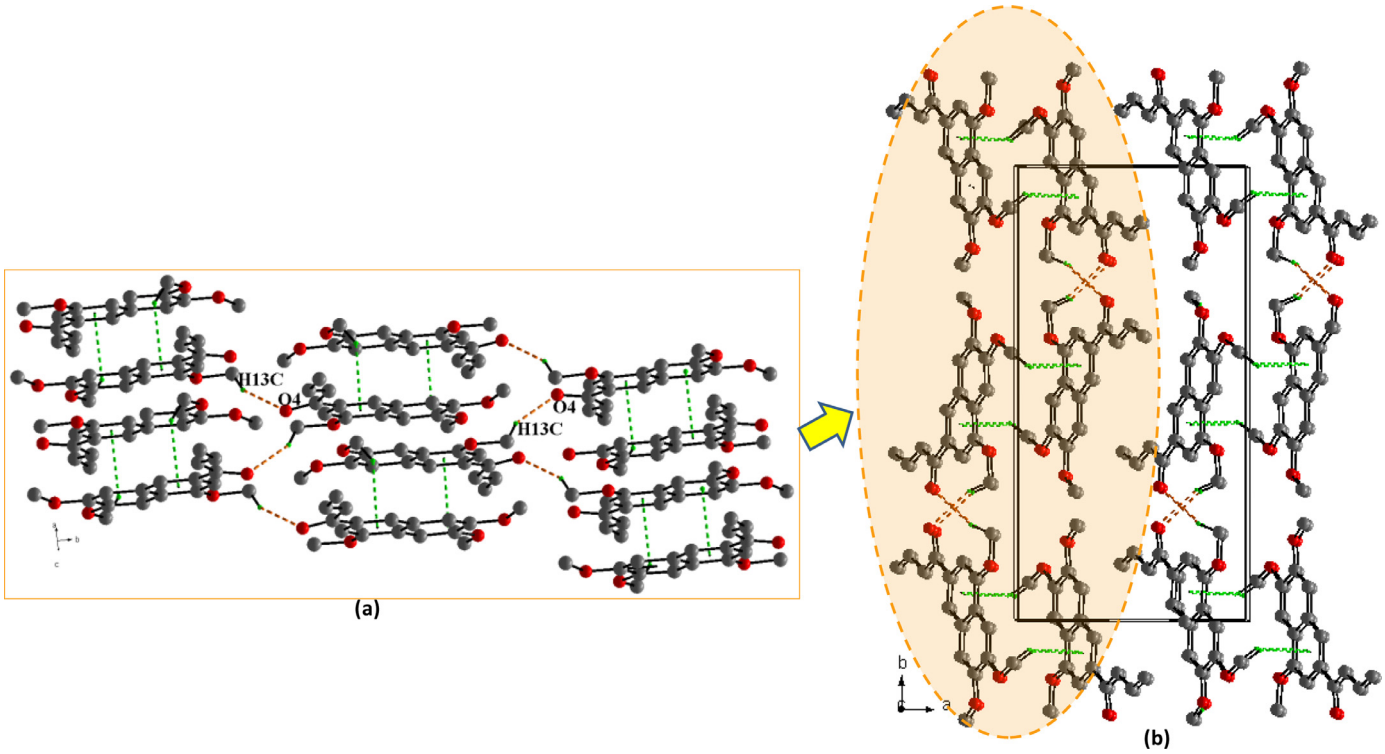


**Fig. 4.** (**a**) Parts of the crystal structure of **5** showing C—H···O hydrogen bond and C—H···$\pi$ interactions and (**b**) view of the supramolecular structure for **5** along the c-axis direction.

130.2, 122.5, 120.4, 108.2, 103.0, 101.5, 61.2, 56.0, 55.9, 55.9, 34.1. HRMS (ESI): *m/z* calcd for $C_{16}H_{20}O_5N$ $[M+H]^+$ 306.1336; found 306.1327.

### 2.1.4. Synthesis of (E)-1-(4,6,7-trimethoxynaphthalen-2-yl)but-2-en-1-one (5)

To a solution of phosphonate **3** (0.290 g, 0.68 mmol, 1 equiv.) in THF (7 mL) was added in one portion $Ba(OH)_2$ (0.161 g, 0.85 mmol, 1.25 equiv.) at room temperature. After 30 min, a solution of ethanol (0.030 g, 38 µL, 0.68 mmol,1 equiv.) in THF/ $H_2O$ 40:1 (7 mL) was slowly added at room temperature. After 1 h, the reaction mixture was quenched with an aqueous solution of ammonium chloride and extracted three times with EtOAc. Then the organic layer was dried over $MgSO_4$, and concentrated under vacuum. Purification by column chromatography on silica gel (10% EtOAc /hexane) furnished the desired compound as a pale green crystal (0.131 g, 67% yield). $R_f$ = 0.46 (30% EtOAc/hexane); mp: 149-150°C.

IR $\nu_{max}$ ($cm^{-1}$): 1661, 1609, 1582, 1510, 1481, 1259, 1180, 1161, 1011, 849, 833, 729. $^1H$ NMR (400 MHz, Acetone-$d_6$, $\delta$ ppm, *J* Hz): $\delta$ = 8.12 (s, 1H), 7.52 (s, 1H), 7.42 (s, 1H), 7.33 (s, 1H), 7.28 (dd, *J* = 15.5, 1.5 Hz, 1H), 7.10-7.02 (m, 1H), 4.05 (s, 3H), 3.96 (s, 3H), 3.95 (s, 3H), 2.00 (dd, *J* = 6.8, 1.5 Hz, 3H). $^{13}C$ NMR (100 MHz, Acetone-$d_6$): $\delta$ = 189.3, 155.6, 152.3, 152.0, 143.9, 135.0, 130.3, 127.9, 124.2, 122.7, 108.9, 101.7, 101.2, 56.0 (× 3), 18.5. HRMS (ESI): *m/z* calcd for $C_{17}H_{19}O_4$ $[M+H]^+$ 287.1278; found 287.1271.

### 2.1.5. Synthesis of 1-(4,6,7-trimethoxynaphthalen-2-yl)hexan-1-one (6)

To a suspension of Mg turnings (0.472 g, 19.54 mmol) in dry THF (12 mL) were added a small piece of iodine and 1-bromopentane (1.53 mL, 12.37 mmol). The mixture was heated by a heat gun and stirred for 0.5 h. To the resulting Grignard reagent was added amide N,4,6,7-tetramethoxy-N-methyl-2-naphthamide **4** (0.250 g, 0.82 mmol) in THF (5 mL) at room temperature, and the mixture was stirred for 0.5 h. The reaction was quenched with saturated $NH_4Cl$ and extracted with AcOEt. The organic layer was washed with brine, dried over $MgSO_4$, and evaporated. The residue was chromatographed on silica gel to afford 1-(4,6,7-trimethoxynaphthalen-2-yl)hexan-1-one **6** (0.241 g, 93% yield) as white crystals. $R_f$ = 0.33 (30% EtOAc/hexane); mp: 109-110°C.

IR $\nu_{max}$ ($cm^{-1}$): 1674, 1510, 1481, 1464, 1427, 1404, 1261, 1219, 1159, 1011, 849, 725, 717. $^1H$ NMR (400 MHz, $CDCl_3$, $\delta$ ppm, *J* Hz): $\delta$ = 7.93 (s, 1H), 7.52 (s, 1H), 7.31 (s, 1H), 7.18 (s, 1H), 4.03 (s, 6H), 4.00 (s, 3H), 3.04 (t, *J* = 7.4 Hz, 2H), 1.77 (qu, *J* = 7.4 Hz, 2H), 1.37 (m, 2H), 0.92 (t, *J* = 7.0 Hz, 3H). $^{13}C$ NMR (100 MHz, $CDCl_3$): $\delta$ = 200.5, 154.8, 151.0, 150.3, 133.6, 129.2, 123.7, 121.6, 107.6, 101.2, 100.3, 56.1, 56.0, 55.7, 38.4, 31.8, 24.7, 22.7, 14.1. HRMS (ESI): *m/z* calcd for $C_{19}H_{25}O_4$ $[M+H]^+$ 317.1747; found 317.1740.

### 2.1.6. Synthesis of 3-(hydroxymethyl)-6,7-dimethoxynaphthalen-1-ol (9)

To a magnetically stirred suspension of lithium aluminum hydride (1.37 g, 36.19 mmol) in THF (50 mL) was added dropwise a solution of ester, Ethyl 4-hydroxy-6,7-dimethoxy-2-naphthoate **1** (6 g, 18.10 mmol) in THF (50 mL) at 0°C. The ensuing mixture was stirred at 0°C for 30 min and then allowed to warm to room temperature. The reaction was stirred at room temperature for 1 h before being cooled to 0°C and quenched by the sequential addition of water (5 mL), saturated aqueous $NH_4Cl$ (10 mL) and water (5 mL). After stirring for 30 min, the reaction mixture was filtered through a glass frit and the aqueous layer was extracted with EtOAC. The combined organic fractions were dried over $MgSO_4$ and concentrated *in vacuo* to provide the title compound **9** (4 g, 94%) as a light yellow solid. $R_f$ = 0.36 (30% EtOAc/hexane); m.p. 220-221°C.

IR $\nu_{max}$ ($cm^{-1}$): 3478, 3198, 1614, 1589, 1493, 1402, 1252, 1207, 1182, 1148, 1016, 997, 972, 847, 768.$^1H$ NMR (400 MHz, DMSO-$d_6$, $\delta$ ppm, *J* Hz): $\delta$ = 9.87 (bs, 1H), 7.38 (s, 1H), 7.17 (s, 1H), 7.12 (s, 1H), 6.75 (s, 1H), 5.15 (bs, 1H), 4.52 (s, 2H), 3.85 (d, *J* = 2.2 Hz, 6H). $^{13}C$ NMR (101 MHz, DMSO-$d_6$, $\delta$ ppm): $\delta$ = 152.0, 149.5, 148.0, 138.9,

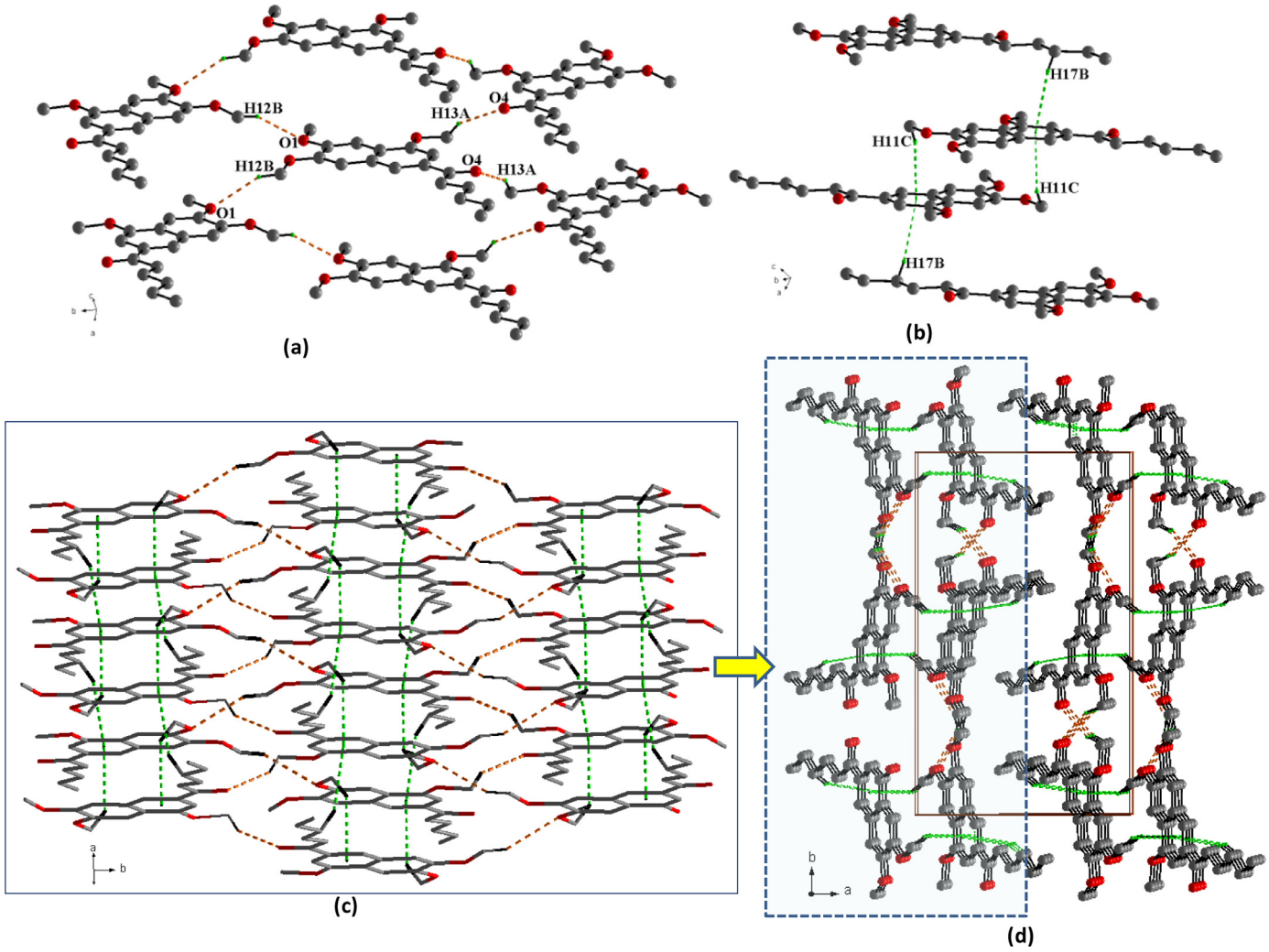


**Fig. 5.** (**a**) C—H…O hydrogen bond interactions in compound **6**, (**b**) C—H…$\pi$ interactions, (**c**) view of the supramolecular structure via C—H···O hydrogen bond and C—H···$\pi$ interactions and (**d**) view of the supramolecular structure for **6** along the c-axis direction.

130.1, 118.6, 114.4, 106.5, 106.9, 101.0, 63.4, 55.3, 55.2. HRMS (ESI): *m/z* calcd for $C_{13}H_{15}O_4$ $[M+H-H_2O]^+$ 217.0859; found 217.0854.

*2.1.7. Synthesis of 4-bromo-3-(hydroxymethyl)-6,7-dimethoxynaphthalen-1-ol (10)*

To a stirred solution of 3-(hydroxymethyl)-6,7-dimethoxynaphthalen-1-ol **9** (3.0 g, 12.81 mmol) in THF (100 mL) at 0°C was added pyridinium tribromide (4.30 g, 13.45 mmol) in five portions over 1 h. Stirring was continued for an additional hour, and water was added to dissolve precipitated pyridinium hydrobromide. The product was extracted with $Et_2O$ and washed twice with 10% $Na_2S_2O_3$. The aqueous layers were extracted once with $Et_2O$ and the combined organics were dried over $MgSO_4$ and concentrated *in vacuo*. The crude residue was purified by column chromatography (50% EtOAc/hexane) on silica gel to afford **10** (3.85 g, 96%) as a yellow solid. $R_f$ = 0.37 (50% EtOAc/hexane); m.p. 200-202°C.

IR $\nu_{max}$ ($cm^{-1}$): 3474, 3289, 1609, 1497, 1393, 1254, 1153, 1030, 984, 845, 777. $^1H$ NMR (400 MHz, DMSO-$d_6$, $\delta$ ppm, *J* Hz): $\delta$ = 10.23 (s, 1H), 7.46 (s, 1H), 7.39 (s, 1H), 7.07 (s, 1H), 5.42 (bs, 1H), 4.63 (s, 2H), 3.91 (s, 3H), 3.89 (s, 3H). $^{13}C$ NMR (101 MHz, DMSO-$d_6$, $\delta$ ppm): $\delta$ = 151.9, 150.7, 148.5, 137.8, 128.1, 119.6, 106.9, 106.8, 106.0, 101.5, 63.3, 55.4, 55.3. HRMS (ESI): *m/z* calcd for $C_{13}H_{14}O_4{}^{79}Br$ $[M+H-H_2O]^+$ 294.9964; found 294.9964.

*2.1.8. Synthesis of 4-bromo-3-(hydroxymethyl)-6,7-dimethoxynaphthalen-1-yl acetate (11)*

To a stirred solution of 4-bromo-3-(hydroxymethyl)-6,7-dimethoxynaphthalen-1-ol **10** (1.0 g, 3.19 mmol) and $K_2CO_3$ (1.32 g, 9.58 mmol) in MeCN (50 mL) under argon atmosphere at room temperature was added acetyl chloride (0.341 mL, 4.79 mmol). The reaction mixture was then stirred at room temperature for 18 h. The reaction was then quenched with water (30 mL) and extracted with EtOAc (3 × 50 mL). The combined organics were washed with brine (20 mL), dried over $MgSO_4$, concentrated under reduced pressure and purified by column chromatography (20% EtOAc /hexane) to afford the title compound **11** (0.99 g, 87%) as a yellow crystalline solid. $R_f$ = 0.31 (30% EtOAc/hexane); m.p. 153-154°C.

IR $\nu_{max}$ ($cm^{-1}$): 3512, 1744, 1611, 1611, 1510, 1485, 1435, 1369, 1310, 1259, 1204, 1180, 1142, 845, 777. $^1H$ NMR (400 MHz, $CDCl_3$, $\delta$ ppm, *J* Hz): $\delta$ =7.51 (s, 1H), 7.28 (s, 1H), 7.02 (s, 1H), 5.28 (s, 1H), 4.85 (s, 2H), 4.03 (s, 3H), 3.98 (s, 3H), 2.44 (s, 3H). $^{13}C$ NMR (101 MHz, $CDCl_3$, $\delta$ ppm): $\delta$ = 169.4, 151.2, 150.4, 145.2, 136.3, 129.2, 122.5, 117.2, 116.6, 106.3, 100.0, 65.4, 56.1, 56.0, 21.14. HRMS (ESI): *m/z* calcd for $C_{15}H_{16}O_5{}^{79}Br$ $[M+H-H_2O]^+$ 337.0070; found 337.0057.

*2.1.9. Synthesis of (1-bromo-4-((tert-butyldimethylsilyl)oxy)-6,7-dimethoxynaphthalen-2-yl)methanol hydrate (12)*

A solution of 4-bromo-3-(hydroxymethyl)-6,7-dimethoxynaphthalen-1-ol **10** (800 mg, 2.55 mmol), imidazole (347.8 mg, 5.11 mmol), 4-(dimethylamino)pyridine (156.0 mg, 1.28 mmol), and TBSCl (577.5 mg, 3.83 mmol) in $CH_2Cl_2$ (50 mL) was stirred at room temperature for 8 h. The reaction was then quenched with water (30 mL) and extracted with $CH_2Cl_2$ (3 × 50 mL). The combined organics were washed with brine (20 ml), dried over $MgSO_4$, concentrated under reduced pressure and purified by column chromatography (5% EtOAc /hexane) to afford the title compound **12** (850 mg, 78%) as a yellow crystalline solid. $R_f$ = 0.44 (20% EtOAc/hexane); m.p. 119-120°C.

IR $\nu_{max}$ ($cm^{-1}$): 3536, 1601, 1512, 1438, 1431, 1317, 1258, 1207, 1157, 1043, 833, 781. $^1$H NMR (400 MHz, $CDCl_3$, $\delta$ ppm, *J* Hz): $\delta$ =7.49 (s, 1H), 7.46 (s, 1H), 6.93 (s, 1H), 4.86 (s, 2H), 4.03 (s, 3H), 3.98 (s, 3H), 2.27 (bs, 1H), 1.10 (s, 9H), 0.27 (s, 6H). $^{13}$C NMR (101 MHz, $CDCl_3$, $\delta$ ppm): 150.9, 150.5, 149.3, 136.2, 129.2, 123.6, 112.1, 112.0, 106.1, 101.9, 66.0, 56.0, 55.9, 25.9 (× 3), 18.5, -4.1 (× 2). HRMS (ESI): *m/z* calcd for $C_{19}H_{27}O_4Si^{79}Br$ [M+H-$H_2O$] $^+$ 409.0829; found 409.0814.

*2.2. Single crystal X-ray data collection*

For all crystal structure determinations, the X-ray intensity data were collected on a Bruker *APEX*-II CCD diffractometer with Mo*Kα* radiation (λ= 0.71073Å) monochromated by graphite at 173K. The following software was used: Frame integration, Bruker SAINT software package and data were corrected for Lorentz-Polarization effects and for absorption by the numerical semi-empirical method implanted in SADABS [40]. The structures were solved by direct methods using SHELXT-2014/5 [41] and refined by the full matrix least-square method on $F^2$ to convergence using the SHELXL-2018/3 program [42]. Anisotropic thermal factors were assigned to all the non-hydrogen atoms. The C-bound H atoms were geometrically placed (C—H = 0.93–0.98 Å) and refined as riding with $U_{iso}$(H) = 1.2–1.5$U_{eq}$(C). The O-bound H-atom in the hydroxyl group and the water molecule for compounds **11** and **12,** respectively, were located in a difference Fourier map and refined freely. Crystal data, data collection and structure refinement details for **5, 6, 8, 11, 12, 14** and **17** are summarized in Table 1. Details on the crystallographic studies, as well as atomic displacement parameters, are given as Supporting Information in the form of cif files. Visualization of the structures was made with the Diamond program [43].

*2.3. Hirshfeld surface and 2D fingerprint plots*

The Hirshfeld surfaces calculated for compounds **5, 6, 8, 11, 12, 14** and **17** provide additional information on the distinctive contributions made to the molecular packing by the independent molecules. Thus, a Hirshfeld surface analysis [44] and the associated two-dimensional fingerprint plots [45] were performed using Crystal Explorer 17.5 [46] to figure out the normalized contact distance ($d_{norm}$), which depends on contact distances to the closest atoms outside ($d_e$) and inside ($d_i$) the surface. The electrostatic potential was generated using the STO-3G basis set at the Hartree-Fock of theory for all the compounds investigated.

*2.4. Quantum chemical calculations*

Optimization of the geometry of all the molecules was performed by means of the Gaussian 09 W program and GaussView molecular visualization software [47,48], based on density functional theory DFT, using Beck's three parameters hybrid functional

**Table 1**
Crystal Data, Summary of Intensity Data Collection, and Structure Refinement.

| | Compound **5** | Compound **6** | Compound **8** | Compound **11** | Compound **12** | Compound **14** | Compound **17** |
|---|---|---|---|---|---|---|---|
| Chemical formula | $C_{17}H_{18}O_4$ | $C_{19}H_{24}O_4$ | $C_{17}H_{17}BrO_6$ | $C_{15}H_{15}BrO_5$ | $C_{19}H_{27}BrO_4Si.H_2O$ | $C_{16}H_{13}F_3O_7S$ | $C_{17}H_{14}F_3NO_7S$ |
| $M_r$ | 286.31 | 316.38 | 397.21 | 355.18 | 445.42 | 406.32 | 433.35 |
| Crystal system, space group | Monoclinic, $P2_1/c$ | Monoclinic, $P2_1/c$ | Triclinic, $P\bar{1}$ | Triclinic, $P\bar{1}$ | Triclinic, $P\bar{1}$ | Triclinic, $P\bar{1}$ | Triclinic, $P\bar{1}$ |
| Temperature (K) | 173 | 173 | 173 | 173 | 173 | 203 | 203 |
| *a*, *b*, *c* (Å) | 10.6316 (13), 20.197 (3), 6.9437 (9) | 11.8171 (11), 19.9271 (18), 7.1032 (7) | 7.8624 (4), 10.2126 (6), 21.1840 (11) | 8.5050 (6), 9.5246 (6), 9.6303 (6) | 7.7048 (5), 11.4248 (7), 12.7403 (7) | 7.6836 (5), 10.2095 (6), 11.3333 (6) | 8.2724(7), 11.5747((8), 20.2131(16) |
| *α*, *β*, *γ* (°) | 90, 105.356 (4), 90 | 90, 94.925(4), 90 | 98.171 (3), 99.499 (3), 94.642 (3) | 87.034 (4), 76.733 (4), 71.621 (4) | 97.973 (3), 104.743 (3), 94.018 (3) | 107.791 (2), 96.279 (3), 95.088 (3) | 94.633(4), 93.035(4), 106.425(4) |
| *V* (Å$^3$) | 1437.8 (3) | 1666.5 (3) | 1651.11 (16) | 720.39 (8) | 1067.55 (11) | 834.42 (9) | 1844.5(3) |
| *Z* | 4 | 4 | 4 | 2 | 2 | 2 | 4 |
| Radiation type | Mo *Kα* | Mo *Kα* | Mo *Kα* | Mo *Kα* | Mo *Kα* | Mo *Kα* | Mo *Kα* |
| $\mu$ ($mm^{-1}$) | 0.09 | 0.09 | 2.52 | 2.87 | 2.01 | 0.27 | 0.25 |
| Crystal size (mm) | 0.52 × 0.47 × 0.15 | 0.51 × 0.26 × 0.11 | 0.27 × 0.11 × 0.05 | 0.21 × 0.14 × 0.04 | 0.24 × 0.21 × 0.19 | 0.59 × 0.47 × 0.13 | 0.45 × 0.29 × 0.14 |
| Diffractometer | Bruker *APEX*-II CCD | Bruker *APEX*-II CCD | Bruker *APEX*-II CCD | Bruker *APEX*-II CCD | Bruker *APEX*-II CCD | Bruker *APEX*-II CCD | Bruker *APEX*-II CCD |
| Absorption correction | Numerical (*SADABS*, Bruker, 2001). | Numerical (*SADABS*, Bruker, 2001). | Numerical (*SADABS*, Bruker, 2001). | Numerical (*SADABS*, Bruker, 2001). | Numerical (*SADABS*, Bruker, 2001) | Numerical (*SADABS*, Bruker, 2001). | Numerical (*SADABS*, Bruker, 2001). |
| $T_{min}$, $T_{max}$ | 0.907, 1.000 | 0.887, 1.000 | 0.564, 0.921 | 0.636, 0.939 | 0.537, 0.613 | 0.703, 1.000 | 0.723, 1.000 |
| No. of measured, independent and observed [$I > 2\sigma(I)$] reflections | 91276, 4620, 3842 | 120691, 5547, 3977 | 105418, 6046, 4500 | 57186, 5015, 3311 | 87118, 7108, 5905 | 153228, 6223, 5509 | 130444, 9532, 6862 |
| $R[F^2 > 2\sigma(F^2)]$, $wR(F^2)$, *S* | 0.041, 0.129, 1.04 | 0.043, 0.135, 1.02 | 0.033, 0.071, 1.01 | 0.041, 0.086, 1.02 | 0.026, 0.068, 1.05 | 0.046, 0.140, 1.08 | 0.042, 0.120, 1.02 |
| Data / restraints / parameters | 4620/0/194 | 5547/0/212 | 6046/0/441 | 5015/0/197 | 7108/3/254 | 6223/0/247 | 9532/0/529 |
| H-atom treatment | H-atom parameters constrained | H-atom parameters constrained | H-atom parameters constrained | H atoms treated by a mixture of independent and constrained refinement | H atoms treated by a mixture of independent and constrained refinement | H-atom parameters constrained | H-atom parameters constrained |
| $\Delta\rho_{max}$, $\Delta\rho_{min}$ (e Å$^{-3}$) | 0.43, -0.26 | 0.39, -0.21 | 0.38, -0.39 | 0.79, -0.89 | 0.39, -0.26 | 0.70, -0.40 | 0.67, -0.40 |

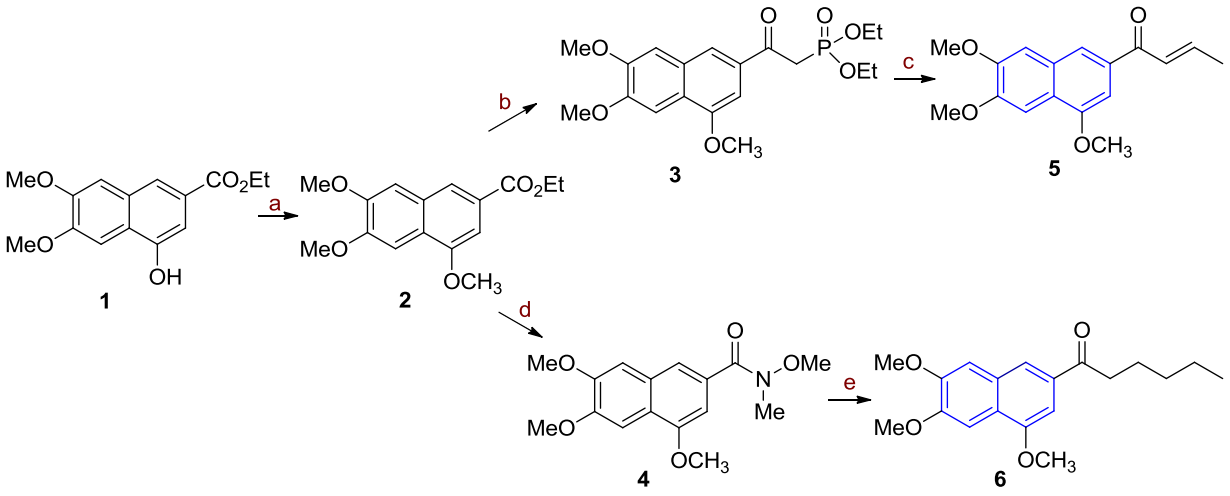


**Scheme 1.** Conditions for synthesis of compounds **5** and **6**. Reagents and conditions: a) $(CH_3)_2SO_4$, $K_2CO_3$, acetone, reflux, 12 h, 95%; b) n-BuLi, THF, -78°C, $(EtO)_2P(O)Me$, 98%; c) $C_2H_4O$, $Ba(OH)_2$ / H2O, THF/$H_2O$ (40:1), 20°C, 2 h, 68%; d) 5% KOH/MeOH:$H_2O$ (19:1), 60°C, 3 h, then $C_2H_8ClNO$, CDI, $CH_2Cl_2$, 69% overall yield; e) $C_5H_{11}MgBr$ THF, 93%.

exchange [49], with 6-311G (d, p) basis sets and Lee-Yang-Parr correlation functional (B3LYP) [50,51]. Molecular Electrostatic Potential (MEP) maps allowed us to visualize the variably charged regions of all the molecules (**5, 6, 8, 11, 12, 14** and **17**).

## 3. Results and discussion

### 3.1. Synthesis and characterization

The synthetic route followed for the preparation of compounds **5** and **6** is outlined in Scheme 1. The starting compound ethyl 4-hydroxy-6,7-dimethoxy-2-naphthoate **1** was synthesized according to previously reported procedures [39] using 3,4-dimethoxy benzaldehyde and diethyl succinate by Stobbe condensation and was obtained in a 65% yield over two steps followed by reaction with dimethyl sulphate to give compound **2** in an excellent yield of 92%. Reaction with diethyl methylphosphonate in the presence of butyl lithium led to phosphonate **3** in a 98% yield. Horner-Wadsworth-Emmons (HWE) olefination with ethanal afforded compound **5** in 68% yield. Keto compound **6** was prepared in two steps: first, compound **2** was hydrolyzed to the corresponding carboxylic acid which was transformed to the Weinreb amide **4** by reaction with N-methoxy methylamine in the presence of CDI [52-55], then, the reaction of **4** with pentyl magnesium bromide [56] produced compound **6** in 93% yield (Scheme 1).

The synthetic route followed for the preparation of compounds **8** [38], **11** and **12** is depicted in Scheme 2. As previously reported the synthetic pathway of compounds **7** [38] and **10** was based on the regioselective bromination of naphthalene core. This bromination is affected by the brominating agents and solvents used, together with the substituents on the naphthalene system [57-59]. The best conditions tested were on one hand, the regioselective bromination of the naphthol system **1** with pyridinium tribromide at 0°C in THF, which gave ester **7** in excellent yield, this was then acetylated to **8** with acetyl chloride in good yield [38] (Scheme 2). Naphthol **1** was reduced to **9** by lithium aluminium hydride [60] and the reaction of **9** with pyridinium tribromide [59] gave the 1-bromo compound **10** in excellent yield. The resulting **10** was followed by acetylation [61] and tert-butyldimethylsilylation [62] of the phenol afforded the protected naphthols **11** and **12** respectively (Scheme 2).

As indicated in Scheme 3, according to the published procedure [38] our starting material for the preparation of compound **14** [38] was ethyl 4-hydroxy-6,7-dimethoxy-2-naphthoate **1**. The chloroformylation procedure [63] of starting ester **1**, resulted in the formation of the desired lactone ring **13** [38], which was followed by treatment with trifluoromethane sulfonic-anhydride [64] to give lactone **14** in a good yield of 91% (Scheme 3).

The synthetic utility of **8** as a building block for the novel cyano derivative **16** [38] was investigated as outlined in Scheme 4 [38]. Thus, the reaction of **8** with NBS in dry DMF [57] afforded the dibromo compound **15** [38] in very good yield. The reaction with CuCN in the presence of L-proline [65] yielded the mono cyano derivative **16** which was finally treated with trifluoromethane sulfonic–anhydride under anhydrous conditions giving the respective sulfonate **17** [38] whose spectral data were in accordance with the structure proposed (see experimental section) (Scheme 4).

All the isolated compounds were characterized by elemental analyses, as well as their spectral data which agree with the proposed structures and are summarized in the synthetic section above. The structures of the crystalline compounds **5, 6, 8, 11, 12, 14** and **17** were confirmed by IR, $^1$H-NMR, $^{13}$C-NMR and LC/HRMS as well as by single crystal structure analyses (see Supporting information).

#### 3.1.1. IR spectral analysis

The IR spectra of the synthesized compounds provided evidence for the presence of all the expected functional groups. The formation of compounds **5** and **6** was confirmed by the appearance of an intense band of the carbonyl group C=O at 1661-1674 $cm^{-1}$. In the IR spectrum of compound **8**, after the formation of the acetate group in the final product **8**, the characteristic strong band of the hydroxyl group of the intermediate compound **7**, which appeared at 3385 $cm^{-1}$ disappeared. Two significant stretching bands associated with carbonyl were observed at 1737 $cm^{-1}$ and 1620 $cm^{-1}$, which correlate with compound **8**. The IR spectrum contained a broad hydroxyl stretching band at 3512 $cm^{-1}$ and one sharp carbonyl band at 1744 $cm^{-1}$, which correlate with compound **11**. In addition the IR spectrum of **12** was devoid of a hydroxyl stretching band at 3536 $cm^{-1}$. The presence of a nitrile group C≡N in compounds **16** and **17** was identified by its absorption band at 2212 and 2220 $cm^{-1}$, respectively. The lactone rings in compounds **13** and **14** were confirmed by their characteristic bands in a region of 1715-1755 $cm^{-1}$.

#### 3.1.2. $^1$H and $^{13}$C NMR spectral analysis

The $^1$H NMR spectra of compounds **5** and **6** show a characteristic signal at $\delta_H$ 4.05 ppm (s), 3.96 ppm (s) and 3.95 ppm (s)

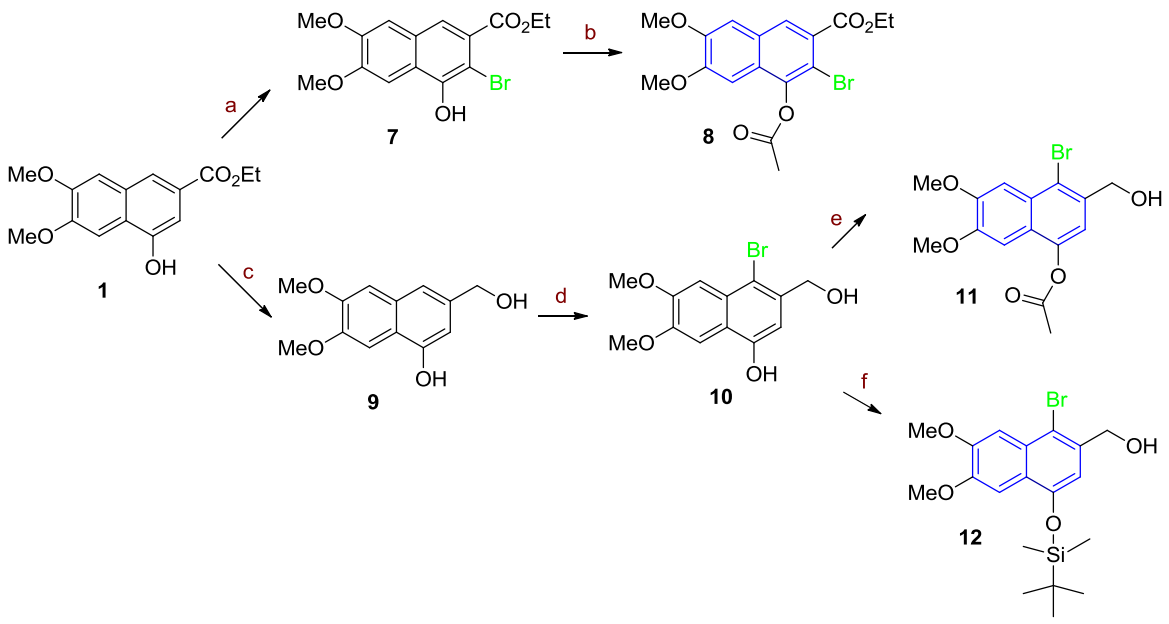

**Scheme 2.** Conditions for synthesis of compounds **8, 11** and **12**. Reagents and conditions: a) $PyrH^+Br_3^-$, THF, 0°C, 1 h, 98%; b) $K_2CO_3$/DMF, 80°C then acetyl chloride, 18 h, 80%; c) $LiAlH_4$, 0°C to rt, 1.5 h, 94%; d) $PyrH^+Br_3^-$, THF, 0°C, 1h, 96%; e) $CH_3COCl$, $K_2CO_3$, MeCN, Ar atm, reflux, 18 h, 87%; f) TBSCl, Imidazole, DMAP, $CH_2Cl_2$, 8 h, rt, 78%.

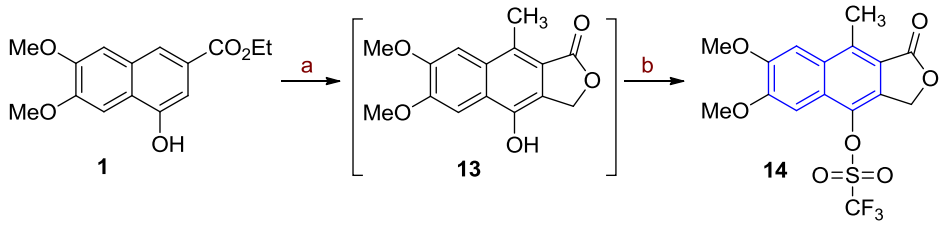

**Scheme 3.** Conditions for synthesis of compound **14**. Reagents and conditions: a) 30% HCHO, 37% HCl, $CH_3CO_2H$, 100°C, 1 h, 40%; $Tf_2O$, $NEt_3$, $CH_3CN$, 0°C to rt, 24 h, 91% [38].

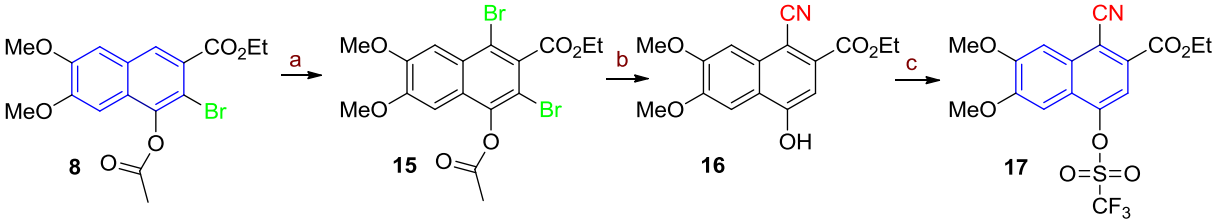

**Scheme 4.** Conditions for synthesis of compound **17**. Reagents and conditions: a) NBS, DMF, rt, 16 h, 86%; b) CuCN, L-Proline, DMF, Argon atm., 150°C, 24 h, 63%; c) $Tf_2O$, $NEt_3$, $CH_3CN$, 0°C to rt, 24 h, 80% [38].

for compound **5** and peaks at $\delta_H$ 4.03 (s), and 4.00 (s) for compound **6**, these peaks corresponded to hydrogen atoms from three methoxy groups. The peaks in the range of 7.18-8.12 ppm are due to the hydrogen atoms bound to the aromatic ring for naphthalene. In addition, the peak at $\delta_H$ 7.28 (dd, $J$ = 15.5, 1.5 Hz, 1H), 7.10-7.02 (m, 1H) was attributed to doublets referring to $\alpha$, $\beta$ unsaturated hydrogens of compound **5**. $^{13}C$ NMR revealed in compounds **5** and **6** three carbons of the methoxy groups at $\delta_C$ (56.0 × 3), 55.7, 56.0 and 56.1 ppm, respectively. In addition, four aromatic olefinic carbons are observed at 101.2, 101.7, 108.9, 122.7 ppm and 100.3 101.2, 107.6, 121.6 ppm for compounds **5** and 6, respectively. The ketone absorbeds at 189.3 and 200.5 ppm, for compounds **5** and **6**, respectively. The olefinic carbons for compound **5** were observed at 127.9 (C$\alpha$) and 143.9 ppm (C$\beta$). The $CH_2$ carbons of the alkyl chain of compound **6** were observed at $\delta_C$ 22.7, 24.7, 31.8 and 38.4 ppm.

The $^1H$ NMR spectrum of compound **8** lacked the hydroxyl proton signal observed in the spectrum of the precursor **7**, but the singlet integrating for three protons at $\delta_H$ 2.51 ppm indicated the presence of the acetate group. Moreover, the ester side chain was also shown to be present by a characteristic quartet at $\delta_H$ 4.42 ppm and an accompanied triplet at 1.42 ppm that integrated for two and three protons respectively. The $^{13}C$ NMR spectrum contained two carbonyl peaks at $\delta_C$ 168.3 and 166.0 ppm corresponded to ester carbonyl and acetate. The two aromatic methoxy groups gave rise to signals at $\delta_C$ 56.0 and 56.1 ppm.

The $^1H$ NMR spectra of compounds **11** and **12** were very indicative of the reaction's success. Additionally, the $^1H$ NMR spectrum of compound **10** contained signals attributed to five protons, which were assigned to ester chain. The emergence of a singlet at $\delta_H$ 4.63 ppm was suggestive of a benzylic $CH_2$ which confirmed that the ester group reduction was successful. The $^{13}$ C NMR spectrum also showed the disappearance of ester carbon signal but a

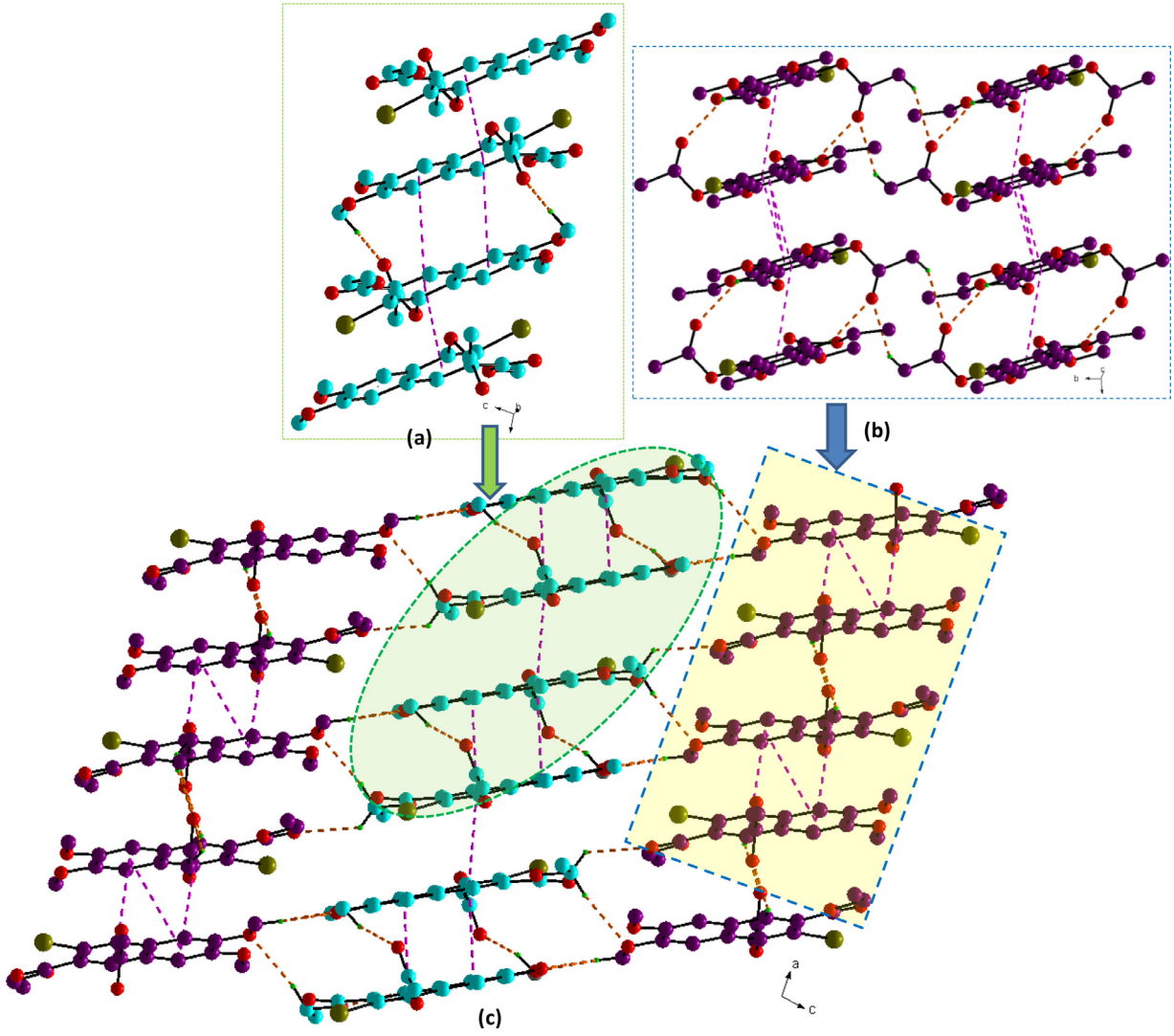


**Fig. 6.** **(a)** dimeric molecular aggregates of *Mol A*, **(b)** dimeric molecular aggregates of *Mol B* and **(c)** Packing and hydrogen-bonding interactions of **8** viewed along the b axis. Hydrogen bonds are drawn as dashed lines and, for the sake of clarity, the H atoms bonded to C atoms have been omitted.

new signal at $\delta_C$ 63.3 ppm was once again indicative of a $CH_2$ group adjacent to an aromatic ring system. The spectral data of the primary alcohol correlate with those reported for compounds **11** and **12**.

The $^1$H NMR of **11** showed the appearance of a new signal at $\delta_H$ 2.44 ppm, that corresponded to the acetate protons. The appearance of the methyl proton at $\delta_H$ 0.23 ppm and 1.13 ppm that integrated for six and nine protons respectively for compound **12**, together with the disappearance of the naphthol proton at $\delta_H$ 5.42 ppm from the starting material **10**. Three new signals were present in the $^{13}$C RMN spectrum of **12**, which were all assigned to the presence of a tert-butyldimethylsilyl protecting group. These signals were at $\delta_C$ 25.9 (× 3) ppm and -4.1 ppm for the methyl carbon atoms, whereas the tertiary carbon atom directly attached to the silicon atom appeared at $\delta_C$ 18.5 ppm.

The $^1$H NMR spectrum of compound **14** closely resembled that of the parent compound **13** as expected, but lacked the signal corresponded to the naphthol proton at $\delta_H$ 9.98 ppm. A distinct singlet signal at $\delta_H$ 5.49 ppm, integrated for two protons $OCH_2$ characteristic of the lactone ring, was also observed. Thus, the methyl group was assigned to the presence of a sharp singlet at $\delta_H$ 2.99 ppm. The $^{13}$C NMR spectrum, showed the appearance of the carbonyl group of lactone at $\delta_C$ 169.4 ppm and the peak at $\delta_C$ 65.5 ppm was due to a $CH_2$ moiety. The presence of methyl signals that were also evident in the $^{13}$C NMR spectrum at $\delta_C$ 12.2 ppm reinforced our proposed structure of compound **14**. The $^1$H NMR spectrum of compound **17** compared very well with that of naphthalene **16** save one difference, namely the disappearance of the OH proton at $\delta_H$ 11.51 ppm for compound **16**. The aromatic region only displayed three naphthalene proton signals as expected. In addition, the $^{13}$C NMR spectrum showed a characteristic signal at $\delta_C$ 97.9 ppm and 99.3 ppm, which refer to the carbons of the nitrile group (C≡N) for compounds **16** and **17**, respectively.

### 3.1.3. Mass spectrometry

The mass spectral data of compounds **5** and **6** confirmed their formation with molecular ion peaks at m/z 287.1271 $[M+H]^+$ for **5** and 317.1740 for **6**, respectively, which was consistent with their molecular formula masses. The HRMS data of compounds **8, 11** and **12** showed intense molecular ion peaks at m/z 397.0261 $[M+H]^+$, 337.0057 $[M+H-H_2O]^+$ and 407.0407 $[M+H-H_2O]^+$ for compounds **8, 11** and **12**, respectively, in agreement with their respective molecular formulae, confirming the presence of bromine in the molecules. Moreover, the HRMS data for the naphthalene lactone **14** and naphthalene **17** were in agreement with the calculated val-

**Table 2**
Hydrogen bonds (Å, °), C—H…$\pi$ and $\pi$…$\pi$ interactions for compounds **5, 6, 8, 11, 12, 14** and **17** Cg1, Cg2, Cg3, Cg4, Cg5 represent the centroids of the, C1–C3/C8-C10, C3–C8, O4/C5/C6/C13/C14, C1B–C3B/C8B-C10B, C3B–C8B rings, respectively.

| | D—H…A | D—H | H…A | D…A or Cg…Cg | D—H…A | Symmetry codes |
|---|---|---|---|---|---|---|
| **5** | C13—H13C···O4 | 0.98 | 2.51 | 3.434(2) | 157 | x,1/2-y,1/2+z |
| | C11—H11A···Cg2 | 0.98 | 2.64 | 3.461(2) | 142 | 2-x,-y,1-z |
| **6** | C12—H12B···O1 | 0.98 | 2.57 | 3.484(2) | 154 | x,-1/2-y,-1/2+z |
| | C13—H13A···O4 | 0.98 | 2.44 | 3.342(2) | 153 | x,1/2-y,1/2+z |
| | C11—H11C···Cg2 | 0.98 | 2.68 | 3.495(2) | 141 | 2-x,-y,1-z |
| | C17—H17B···Cg2 | 0.98 | 2.86 | 3.764(2) | 153 | x,y,-1+z |
| **8** | C7B—H7B···O5B | 0.95 | 2.52 | 3.345(4) | 146 | 1-x,-y,-z |
| | C11B—H11E···O1A | 0.98 | 2.55 | 3.306(4) | 134 | -x,-y,-z |
| | C11B—H11E···O2A | 0.98 | 2.49 | 3.443(4) | 165 | -x, -y, -z |
| | C12A—H12B···O5A | 0.98 | 2.57 | 3.428(4) | 146 | 1-x,1-y,1-z |
| | C14B—H14F···O5B | 0.98 | 2.56 | 3.226(5) | 126 | 1-x,1-y,-z |
| | C16A—H16A···O4B | 0.99 | 2.57 | 3.150(4) | 117 | 2-x,1-y,1-z |
| | C16A—H16B···O1B | 0.99 | 2.49 | 3.470(4) | 171 | 1+x,1+y,1+z |
| | Cg2···Cg2 | | | 3.785(2) | | 2-x,1-y,1-z |
| | Cg4···Cg4 | | | 3.889(2) | | -x,-y,-z |
| | Cg4···Cg5 | | | 3.643(2) | | -x,-y,-z |
| | Cg5···Cg5 | | | 3.873(2) | | 1-x,-y,-z |
| **11** | O4—H4O···O1 | 0.98(4) | 1.99(4) | 2.962(3) | 167 | x,-1+y,z |
| | O4—H4O···O2 | 0.98(4) | 2.57(4) | 3.156(2) | 118 | x,-1+y,z |
| | C5—H5···O4 | 0.95 | 2.47 | 3.328(3) | 150 | 1-x,-y,1-z |
| | C11—H11B···O5 | 0.98 | 2.57 | 3.484(3) | 154 | x,1+y,z |
| | C12—H12A···Cg2 | 0.98 | 2.68 | 3.546(3) | 147 | 1-x,1-y,-z |
| **12** | O1W—H1W···O4 | 0.87(2) | 1.94(2) | 2.801(2) | 171 | 1+x,y,z |
| | O1W—H2W···O1 | 0.84(2) | 2.19(2) | 2.966(2) | 154 | 1-x,1-y,1-z |
| | O1W—H2W···O2 | 0.84(2) | 2.33(2) | 3.001(2) | 137 | 1-x,1-y,1-z |
| | O4—H4···O1W | 0.89(2) | 1.91(2) | 2.791(2) | 174 | 1-x, -y, 1-z |
| | C12—H12A···Cg2 | 0.98 | 2.84 | 3.550(2) | 130 | -x, 1-y, 1-z |
| | Cg1···Cg2 | | | 3.452(1) | | 1-x, 1-y, 1-z |
| | Cg1···Cg1 | | | 3.821(1) | | 1-x, 1-y, 1-z |
| **14** | C11—H11A···O5 | 0.97 | 2.57 | 3.405(2) | 145 | -x,1-y,1-z |
| | C12—H12B···O2 | 0.97 | 2.52 | 3.285(2) | 136 | 1-x,-y,1-z |
| | Cg3···Cg1 | | | 3.509(1) | | -x,1-y,1-z |
| | Cg1···Cg2 | | | 3.858(1) | | -x,1-y,1-z |
| | Cg2···Cg2 | | | 3.607(1) | | -x,1-y,1-z |
| **17** | C11A—H11C···O4A | 0.96 | 2.47 | 2.840(2) | 103 | x, 1+y, z |
| | C11B—H11F···O4B | 0.96 | 2.52 | 2.871(2) | 101 | x, -1+y, z |
| | C12A—H12B···O2B | 0.96 | 2.55 | 3.491(2) | 166 | 1-x, 1-y, 1-z |
| | C12A—H12C···O1B | 0.96 | 2.45 | 3.398(2) | 167 | -1+x, y, z |
| | C12B—H12F···O1A | 0.96 | 2.53 | 3.456(2) | 162 | 1+x, y, z |
| | C16A—H16B···O6B | 0.96 | 2.56 | 3.420(3) | 149 | 2-x,1-y,1-z |
| | Cg2···Cg4 | | | 3.885(1) | | 1-x, 1-y, 1-z |

ues for these compounds at m/z 407.0399 $[M+H]^+$ and $[M+NH_4]^+$ 451.0767, respectively.

### 3.2. Crystal structure of 5, 6, 8, 11, 12, 14 and 17

Crystals of **5, 6, 8, 11, 12, 14** and **17** were obtained by slow evaporation of the solvent system (hexane/ethyl acetate) at room temperature. Compounds **5** and **6** crystallize in the monoclinic system with the $P2_1/c$ space group, while **8, 11, 12, 14** and **17** crystallize in the triclinic system with the $P\bar{1}$ space group. The crystallographic asymmetric-unit contents are shown in Fig. 3. Selected bond lengths and angles of these compounds are also given in Table S1. Hydrogen bond distances and angles together with details of offset C—H···$\pi$ and $\pi$···$\pi$ contacts for all compounds are shown in Table 2. In each of the compounds reported here, the naphthalene unit of the molecules is very planar. The molecular structures of the compounds **5, 6, 8, 11, 12, 14** and **17** are sufficiently similar to be discussed together as they vary only in the substitution pattern on the naphthalene ring at position C4, C5, C6 or C7 atoms. In 6,7-dimethoxynaphthalene, the C1—O1 and C10—O2 bond lengths range from 1.353 to 1.365 Å and 1.350-1.365 Å respectively, indicating the presence of a single bond between oxygen and a $sp^2$ carbon atom, whereas the single bond lengths C11—O1 (1.420-1.432 Å) and C12—O2 (1.422-1.429 Å) are slightly longer due to oxygen and a $sp^3$ carbon.

The supramolecular assembly in the structures reported here is dominated by C—H···O hydrogen bonds for compounds **5, 6, 8, 11, 14, 17** and O—H···O for compounds **11** and **12**. In addition, a weak C—H···$\pi$ interaction involving different donor groups and acceptor $\pi$-ring systems is present in all crystals except compounds **8, 14** and **17**. The $\pi$···$\pi$ contacts between aromatic rings observed in compounds **8, 12, 14** and **17** can be considered to be quite significant.

Compounds **5** and **6** crystallize with a single molecule in the asymmetric parts of the unit cells similar dimensions (Table 1). The geometric parameters of molecules of these two compounds are similar. All non-hydrogen atoms of the molecule are almost coplanar with deviation from the mean plane (r.m.s= 0.077 Å for **5** and 0.069Å for **6**). In both compounds, strong intermolecular C—H···O interactions occur between oxygen atoms of the carbonyl and methoxy groups in position C4 of naphthalene (Figs. 4a and 5a). Other interactions in compound **6** are observed between –$OCH_3$ group protons in position C1 and C10. These contacts are supplementared by the weak C—H···$\pi$ stacking interactions (C11—H11A···**Cg2** 2.64 Å for **5** and C11—H11C···**Cg2** 2.68 Å and C17—H17B···**Cg2** 2.86 Å for **6**) (Figs. 4a and 5b). Thus, the intermolecular interactions give to the formation of the supramolecular crystal packing assembly in all three dimensions (Figs. 4b and 5c-d).

The asymmetric unit of compound **8** consists of two independent molecules, labeled *A* (cyan) and *B* (purple), of similar geom-

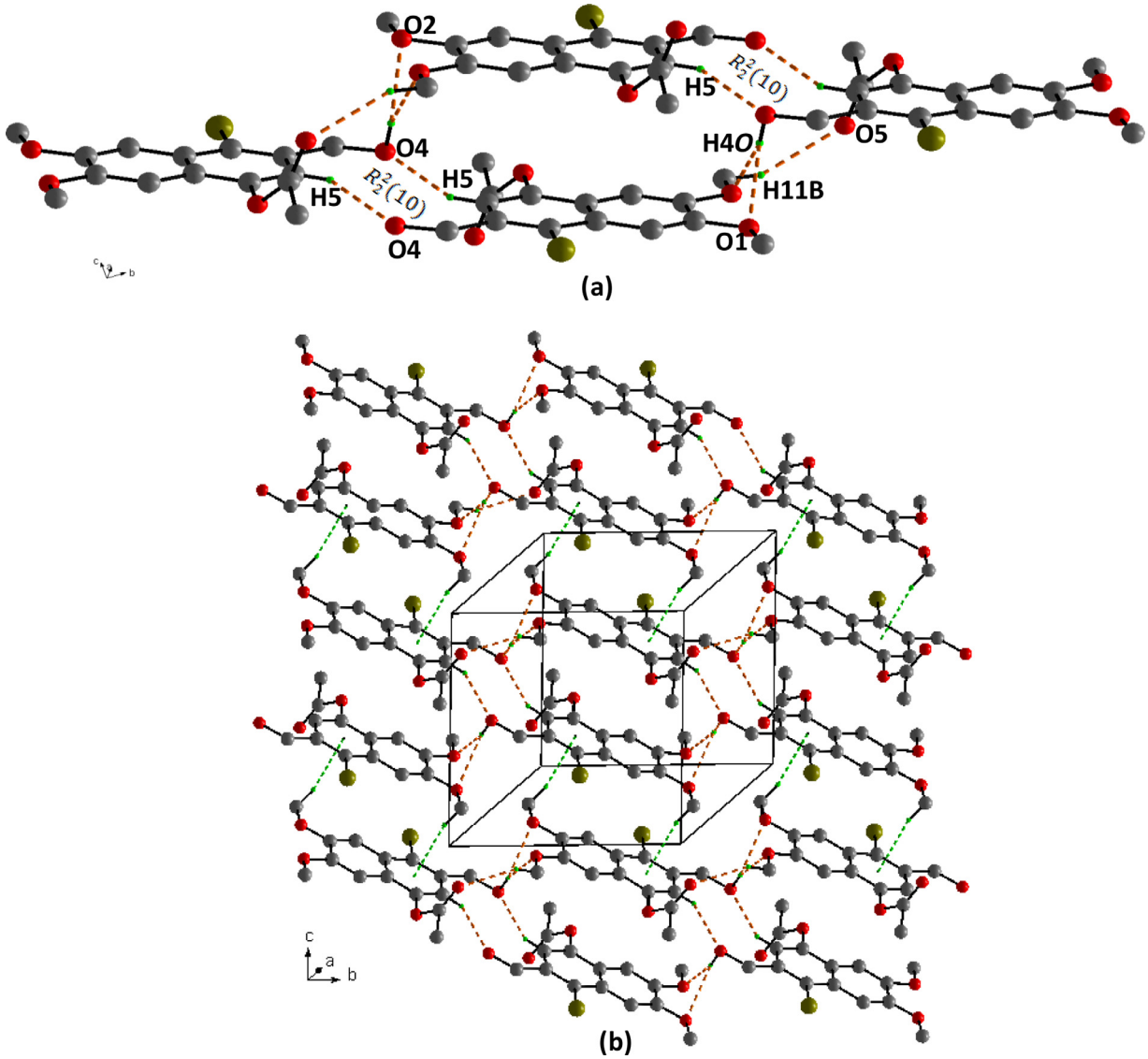


**Fig. 7.** **(a)** dimer hydrogen-bonding motif seen in **11**, linked via C5—H5···O4 which is related to them *via* a bifurcated hydroxy-methoxy O—H···O and methoxy-carbonyl C11—H11B···O5 interactions and **(b)** crystal packing viewed along the a axis. Hydrogen bonds are drawn as dashed orange lines.

etry as shown in Fig. 3. In the crystal structure, each molecule forms an inversion dimer by hydrogen bonds. The dimer of *Mol A* is formed by C12A—H12B···O5A hydrogen bonds, which are connected into a chain along the a-axis through a $\pi-\pi$ stacking interaction between the naphthalene rings [centroid-centroid distance of 3.785(2)Å between C3A-C8A rings] (Table 2 and Fig. 6a). The dimer of *Mol B* formed by C7B—H7B···O5B is associated *via* C14B—H14F···O5B hydrogen bonding into a ribbon that extends approximately parallel to the b-axis through a $\pi-\pi$ stacking interaction between the naphthalene rings [centroid-centroid distance of 3.643(2)Å between C3B-C8B and C1B-C3B/C8B-C10B rings; 3.890(2) between C1B-C3B/C8B-C10B rings] (Table 2 and Fig. 6b). The two sheets of molecules *Mol A* and *Mol B* are connected by C16A—H16A···O4B, C16A—H16B···O1B and C11B—H11E···O1A/O2A hydrogen bonds, forming slabs lying parallel to the ac plane (Fig. 6c).

In compound **11**, the mean plane formed by Br/C1-C12/C15 is almost planar (r.m.s = 0.031) and the acetate group is twisted around this mean plane with 64.58(10)°. In the crystal structure, the molecular packing of the title compound is mainly stabilized by two O—H···O and two C—H···O hydrogen bonds (Fig. 7a, Table 2). Pairs of C5—H5···O4 hydrogen bonds form inversion dimers with an $R_2^2(10)$ ring motif (Fig. 7a). The dimers are additionally linked *via* a bifurcated hydroxy-methoxy O—H···O and methoxy-carbonyl C11—H11B…O5 interactions, forming chains along the b direction. These chains are related by C—H···$\pi$ interactions, leading to the formation of layers parallel to the (011) plane (Fig. 7b).

Compound **12** crystallizes as a monohydrate with two formula units in the asymmetric unit. The naphthalene ring is almost planar with r.m.s= 0.023Å. The Si—C bond length of 1.856(2) to 1.876(2) Å, with an Si—O bond length of 1.665(1) Å indicates an almost tetrahedral geometry around this silicon atom and the angles around the Si atom vary from 103.33(6) to 112.31(8)°. One of the hydrogen bonds donated by water is bifurcated between two acceptors O1 and O2. The oxygen atom of the water molecule acts as acceptor for the hydroxyl hydrogen atom of the neighboring molecule *via* O4—H4···O1W interactions, while the two hydrogen atoms interact with the O atoms of the methoxy and hydroxyl groups of neighboring molecules *via* O1W—H1W···O4, O1W—H2W···O1, O1W—H2W···O2 and O1W—H1W···O4 hydrogen bonds, forming chains parallel to the b axis (Fig .8a). Within the

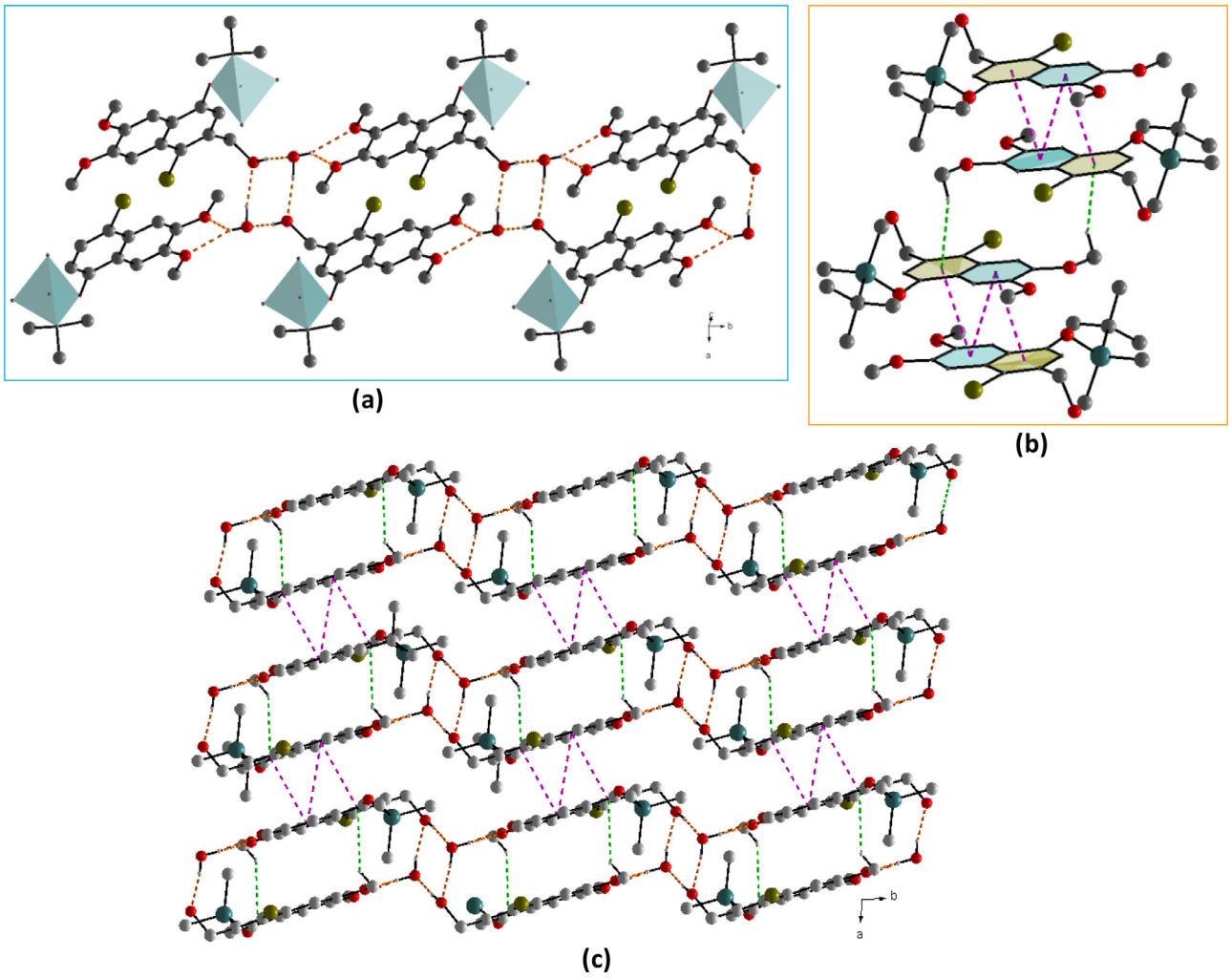


**Fig. 8.** (a) The O—H···O contacts, which connect the molecules into dimers, are shown as dashed lines, (b) C—H···$\pi$ interactions (c) crystal packing of **12**, viewed down [001]. C-bound H atoms have been omitted for clarity.

ribbons are $R_4^4(22)$ as well as $R_4^4(10)$ rings. Weak interactions C—H···$\pi$ and $\pi$···$\pi$ (Fig. 8b) help to consolidate the packing crystal (Fig. 8c).

The molecule structure of compound **14** is illustrated in Fig. 3. In the molecule, the 1,3-dihydronaphtho[2,3-*c*]furan mean plane is approximately planar, with an r.m.s deviation of 0.043 Å. The dihedral angle between the naphthalene and furan rings is 4.31(5)°. The sulfonate group is tilted from the 1,3-dihydronaphtho[2,3-*c*]furan mean plane with 72.00(7)°.

Table S1 shows that the sulfonate group exhibits a tetrahedral geometry with shorter S=O bonds [S1—O6 = 1.417(2)Å and S1—O7 = 1.410(2)Å] when compared to the anionic S—O bond (S1—O3 =1.577(1) Å), as expected. The bond angles between O7—S1—O3 and O7—S1—O3 are 110.58(7) and 110.93(6) respectively. Whereas, 120.6(1)° is for angle between O7—S1—O6. The three C—F distances of the $-CF_3$ group are on average 1.310 Å.

In the crystal **14**, each molecule forms hydrogen-bonded dimers linked by two weak C11—H11A···O5 hydrogen bonds. These dimers are related to them by C12—H12B···O2 hydrogen bonds, resulting in the formation of infinite one-dimensional chains in the direction of the axis (Fig. 9a). In addition, the $\pi-\pi$ stacking interactions observed between the phenyl and phenyl or furan rings with centroid-centroid distances averaging 3.509(1) – 4.000(1) Å (Table 2, Fig. 9b) also contribute to the formation of infinite intermolecular hydrogen bonding forces which play a prominent role in forming the supramolecular system and determining the physicochemical properties. These chains are connected *via* O···F contacts to form layers parallel to ac plane (Fig. 10).

The asymmetric unit of compound **17** contains two independent molecules of similar geometry in *Mol*-A (turquoise) and *Mol*-B (mauve). The naphthalene ring systems are essentially planar with maximum deviations from the mean plane of 0.027° in *Mol-A* and 0.016° in *Mol-B*. The dihedral angle between the fused rings is 2.16(8)° in Mol-A and 1.24(8) in Mol-B. The dihedral angles of the C-(C=O)-O-C-C plane [C6A-(C14A=O4A)-O5A-C15A-C16A and C6B-(C14B=O4B)-O5B-C15B-C16B] and the naphthalene ring are 14.87(7)° and 19.38(8)°, respectively. The three C—S—O angles [C17—S1—O3 (100.0(1)°, C17—S1—O6 (107.3(1)° and C17—S1—O7 (105.4(1)°] and O—S—O angles [O3—S1—O6 (111.3(1)°, O3—S1—O7 (107.8(1)° and O6—S1—O7 (122.6(1) (1)°], indicate that the geometry of the sulfonate group is distorted from an ideal tetrahedral geometry.

In the crystal structure, both molecules from an inversion dimer by hydrogen bonds (C12A—H12C···O1B and C12B—H12F···O1A hydrogen bonds, which are connected by C11A—H11C···O4A and C11B—H11F···O4B hydrogen bonds, forming a chain a along the b-axis (Fig. 11a). These chains are connected by C12A—H12B···O2B and C16A—H16B···O6B hydrogen bonds, forming slabs lying parallel to the ab plane (Fig. 11b). These contacts are strongly supported by extensive $\pi-\pi$ stacking interaction between the naphthalene rings [centroid-centroid distance of 3.885(2)Å between C3A-C8A and C1B-C3B/C8B-C10B rings] (Table 2 and Fig. 11b).

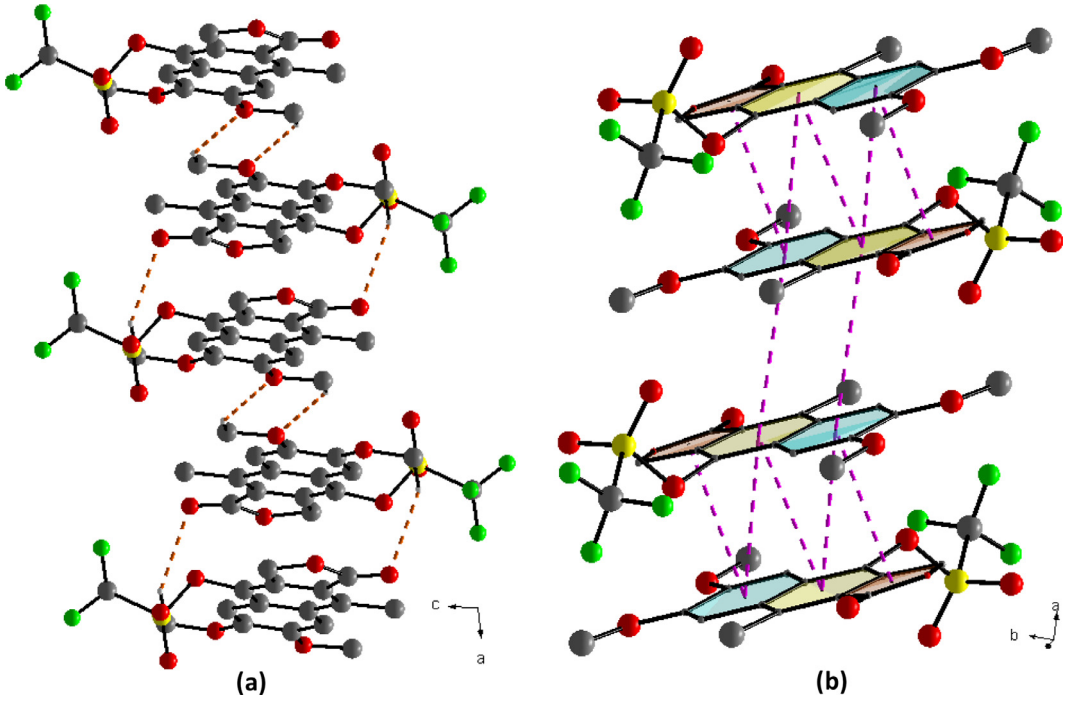


**Fig. 9.** A view of **(a)** one-dimensional chains along the a-axis, showing C—H···O hydrogen bonds, (b).

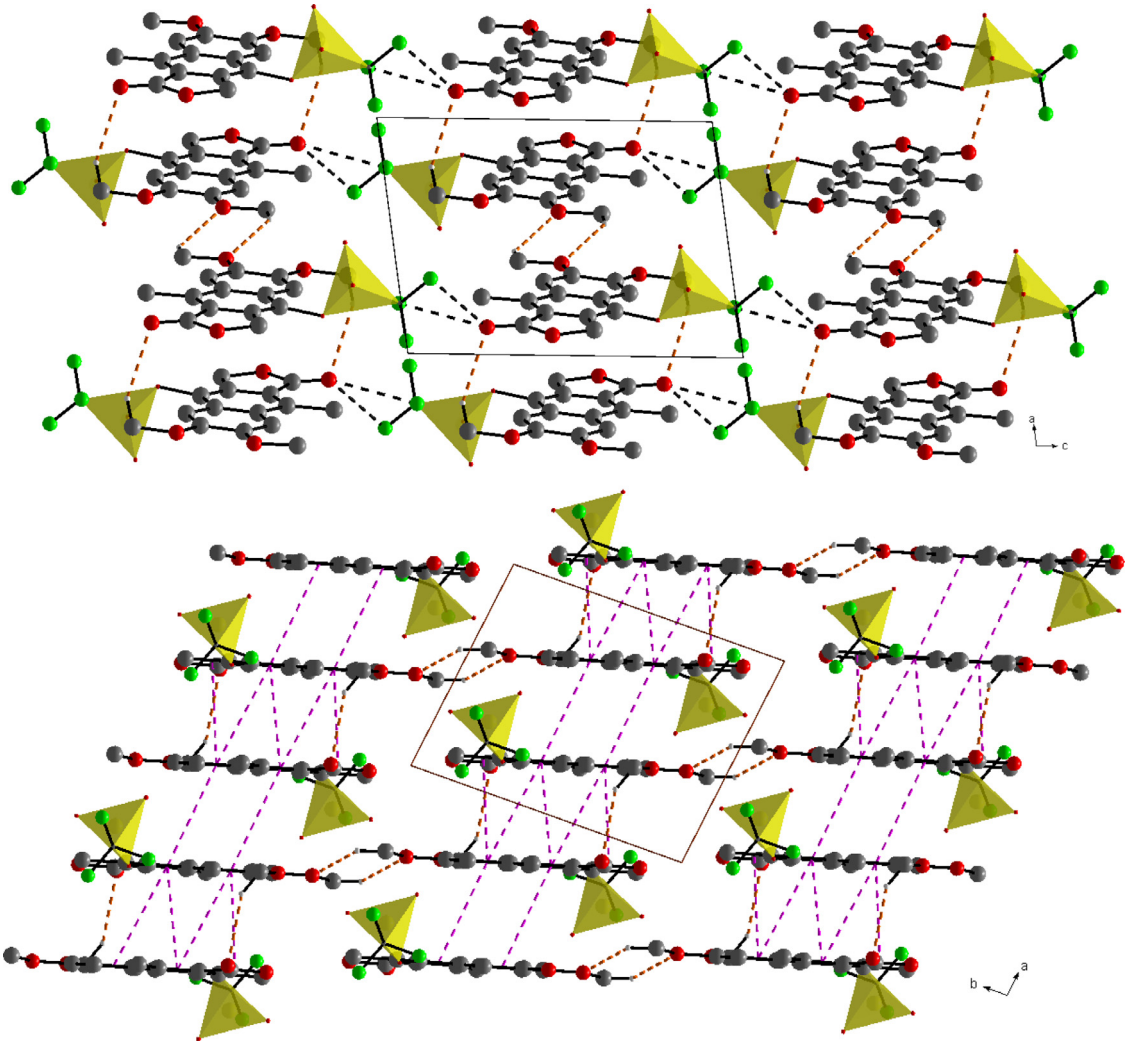


**Fig. 10.** Crystal packing diagram for compound **14** showing C—H···O hydrogen bonds, $\pi-\pi$ stacking interactions and O···F contacts as dashed orange, purple and dark lines, respectively.

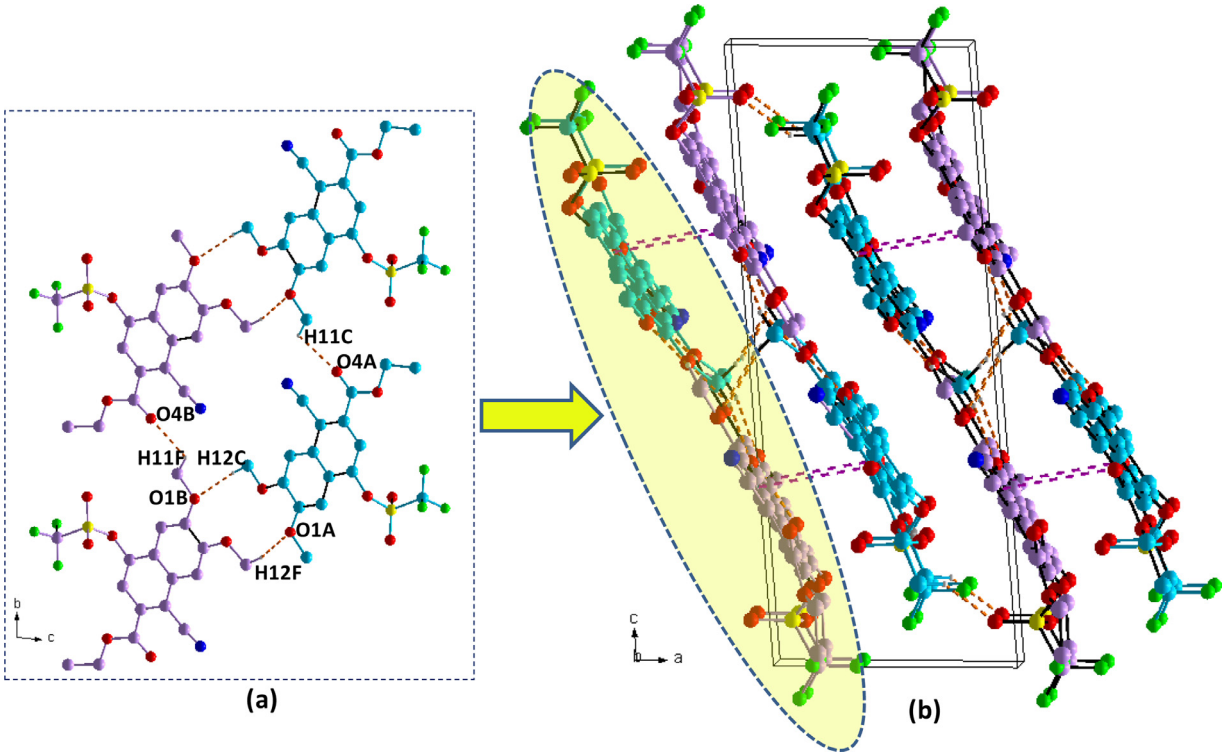


**Fig. 11.** (a) The C—H···O contacts, which connect the molecules into dimers, are shown as dashed lines and (b) crystal packing of **17**, top-down view [010]. C-bound H atoms have been omitted for clarity.

### 3.3. Hirshfeld surface analysis

The Hirshfeld surfaces and 2D fingerprint plots of compounds **5, 6, 8, 11, 12, 14** and **17** were used to obtain information about non covalent interactions in crystal packing. Calculations of the molecular Hirshfeld surfaces (HS) were performed using a standard (high) surface resolution with the three-dimensional $d_{norm}$ surfaces mapped (Fig. 12). The red points represent closer contacts and negative $d_{norm}$ values on the surface corresponded to the C—H···O in compounds **5, 6, 8, 11, 14** and **17** and O—H···O in compounds **11** and **12** (Table 3 and Fig. 12). The light-red spots indicate their involvement in the other intermolecular C—H···$\pi$ (compounds **5, 6, 14** and **8**) and C···C (compounds **8, 14** and **12**). The Hirshfeld surface mapped over the electrostatic potential showed blue regions indicated a positive electrostatic potential, while red spots indicate atoms with a negative electrostatic potential (Fig. 12b).

The overall 2D fingerprint for the main intermolecular contacts of all compounds is shown in Fig. 13. The percentage contributions of the various interatomic contacts to the Hirshfeld surfaces are summarized in Table S2. The contribution was possible for different interactions including H···H and O···H/H···O (for all compounds) and C···H/H···C (in **5, 6, 11** and **12**). The most important interaction was H···H which contributed 49, 57.4, 41.8, 38 and 60.8% overall for **5, 6, 8, 11** and **12** respectively, to stabilizing the crystal packing. This is reflected in Fig. 13b as widely scattered points of high density due to the large hydrogen content of the molecules with the small split tips at $d_e \approx d_i \approx$ 1.15 - 1.25 Å. The higher proportion of hydrogen atoms in structure **12** was afforded by tert-butyldimethylsilyl. These contacts are not visible on the corresponding Hirshfeld surfaces because their distances are longer than the sum of the van der Waals radii. The structures of all molecules are also dominated by O···H/H···O contacts, comprising from 19.3% (**6**) to 33.9% (**14**) (Fig. 13c) of the total Hirshfeld surface areas. These contacts are shown as two symmetrical points on the top, bottom left and right with the shortest $d_e + d_i \approx$ 1.85 – 2.50Å, which is characteristic of the C—H···O hydrogen bond in compounds **5, 6, 8, 11, 14** and **17** and the O—H···O bond in compounds **11** and **12**. The presence of C—H···$\pi$ interactions in

**Table 3**
HOMO–LUMO energies and values of quantum chemical parameters calculated by B3LYP/6-311G (d,p).

| property | Values | | | | | | |
|---|---|---|---|---|---|---|---|
| | 5 | 6 | 8 | 11 | 12 | 14 | 17 |
| $E_T$ ($eV$) | -26105.27 | -28277.94 | -100200.05 | -96046.65 | -108300.33 | -50105.98 | -52648.39 |
| $E_{HOMO}$ ($eV$) | -5.600 | -5.638 | -6.012 | -5.854 | -5.675 | -6.371 | -6.590 |
| $E_{LUMO}$ ($eV$) | -1.812 | -1.531 | -1.612 | -1.299 | -1.162 | -2.026 | -2.568 |
| $\Delta E_{(LUMO-HOMO)}$ ($eV$) | **3.788** | **4.107** | **4.400** | **4.555** | **4.513** | **4.345** | **4.022** |
| Global hardness ($\eta$) | 1.894 | 2.053 | 2.200 | 2.277 | 2.256 | 2.172 | 2.011 |
| Softness ($\xi$) | 0.264 | 0.243 | 0.227 | 0.219 | 0.221 | 0.230 | 0.249 |
| Chemical potential ($\mu$) | 3.706 | 3.584 | 3.812 | 3.576 | 3.418 | 4.198 | 4.579 |
| Electrophilicity ($\psi$) | 3.626 | 3.122 | 3.299 | 2.801 | 2.583 | 4.054 | 5.221 |
| Electronegativity ($\chi$) | -3.706 | -3.584 | -3.812 | -3.576 | -3.418 | -4.198 | -4.579 |
| Dipole moment (D) | 2.319 | 2.666 | 4.568 | 3.504 | 4.418 | 4.909 | 3.584 |

$\eta$=1/2[$E_{LUMO}$-$E_{HOMO}$], $\xi$=1/2$\eta$, $\mu$= -[1/2($E_{LUMO}$+$E_{HOMO}$)], $\psi = \mu^2/2\eta$, $\chi = -\mu$

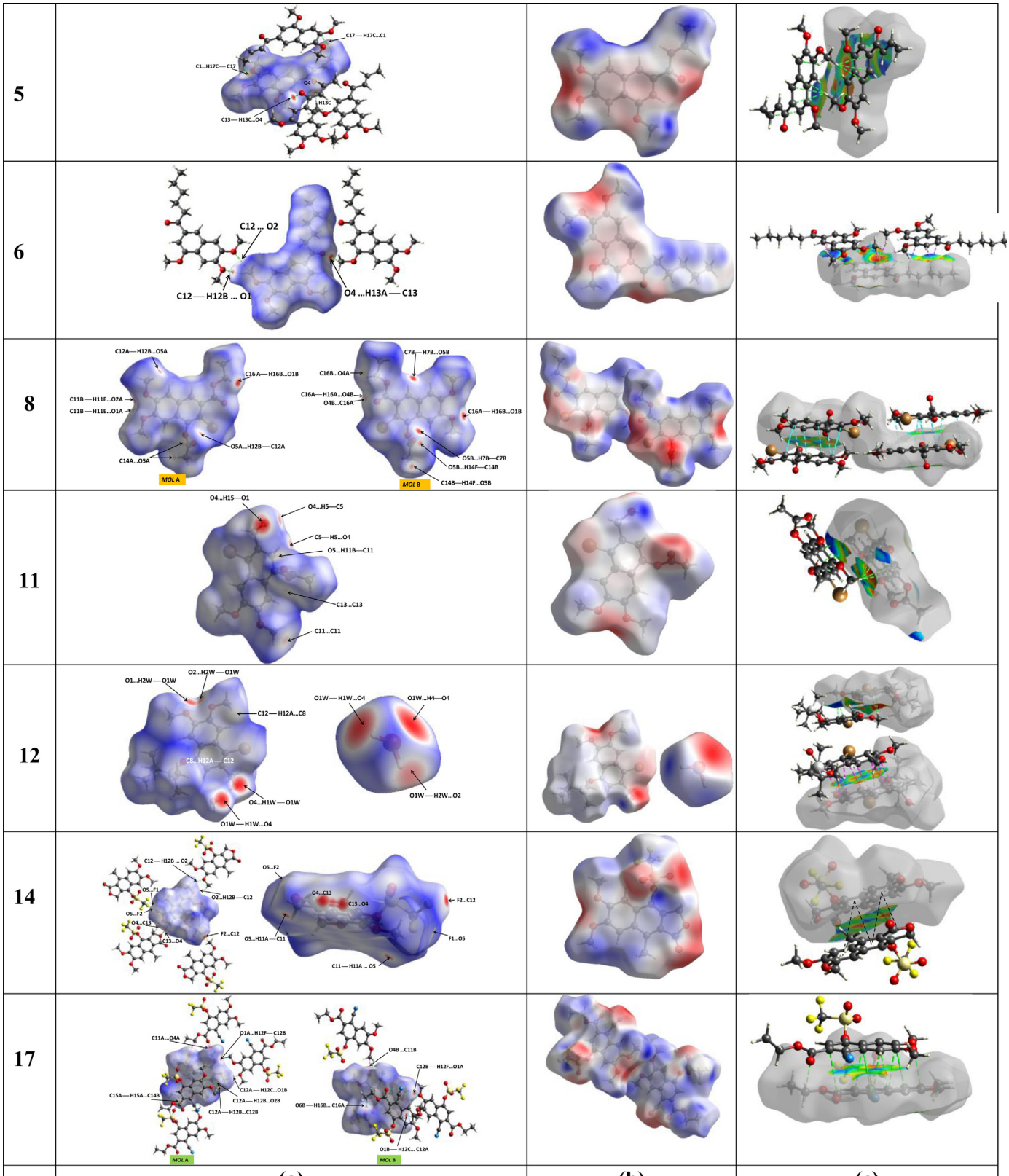


**Fig. 12.** View of the three-dimensional Hirshfeld surface of **5, 6, 8, 11, 12, 14** and **17** plotted over (a) $d_{norm}$, (b) electrostatic potential and (c) shape-indexed features showing C—H···$\pi$ or $\pi$…$\pi$ interactions through dashed lines.

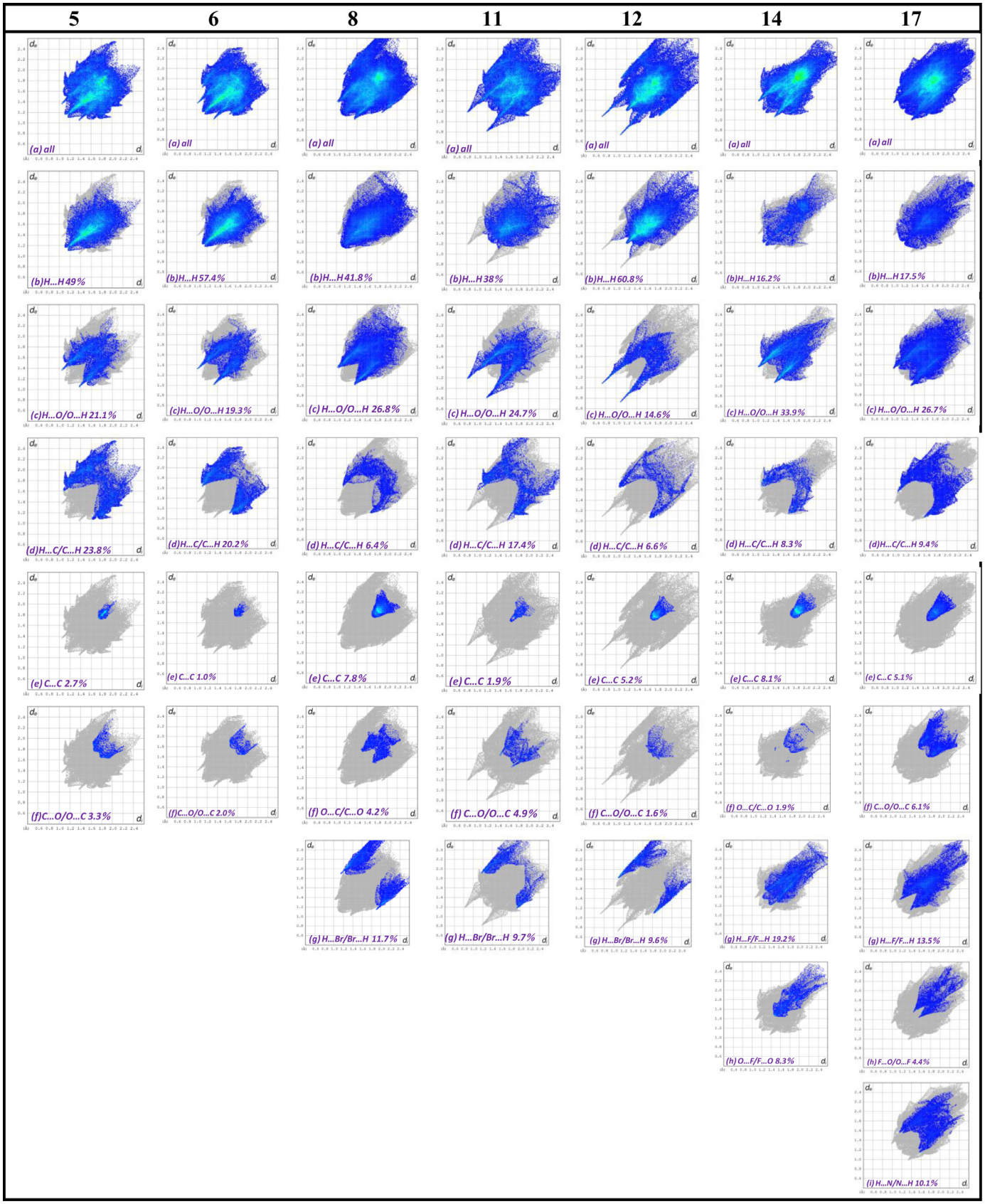


**Fig. 13.** Relative contributions of intermolecular contacts to the Hirshfeld surface area in **5, 6, 8, 11, 12, 14** and **17** and 2D fingerprint plots of observed contacts.

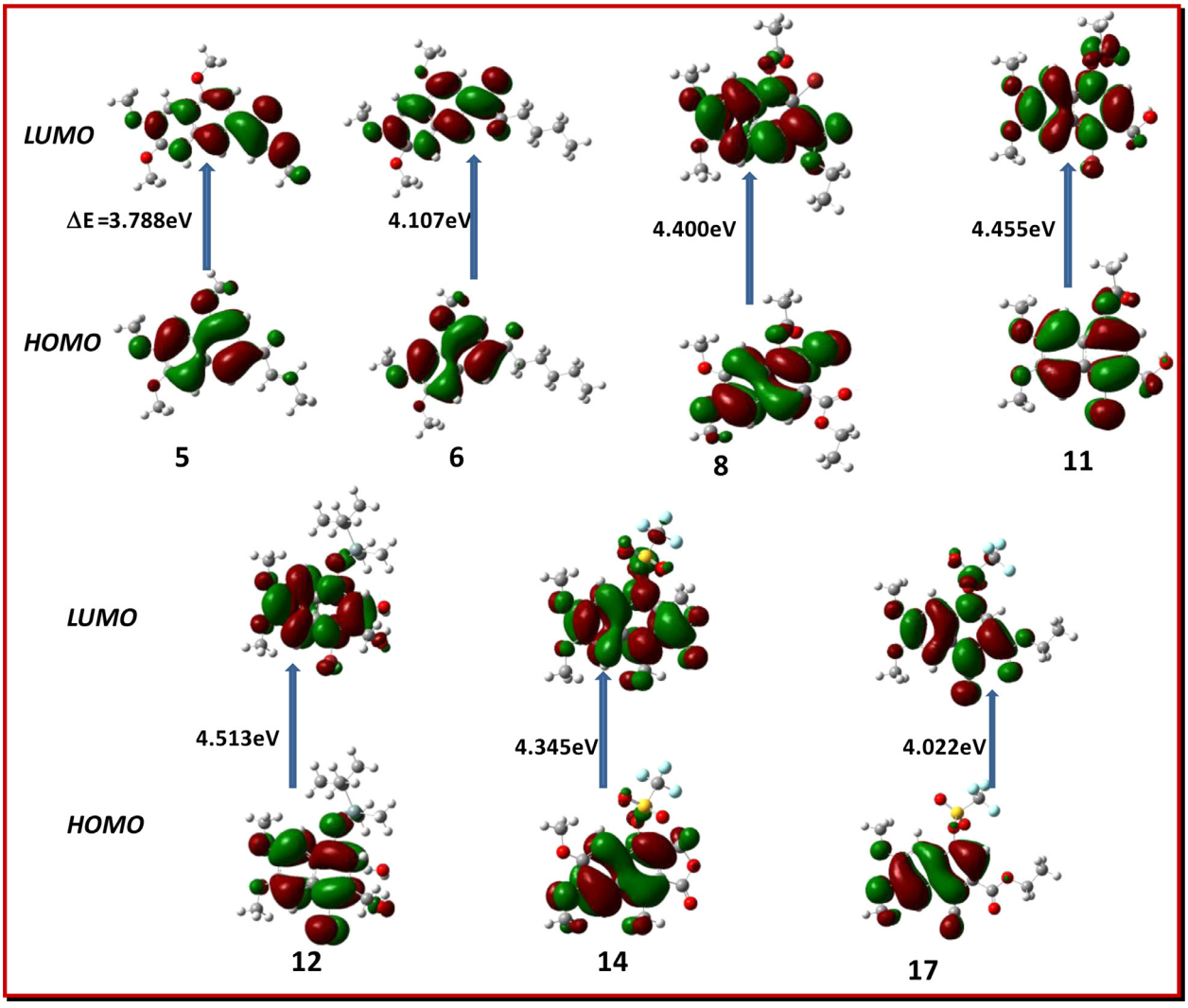


**Fig. 14.** HOMO and LUMO surfaces of **5, 6, 8, 11, 12, 14** and **17** at the B3LYP/6-311G(d,p) level of theory.

the structures **5, 6, 11** and 1**2** is indicated by the pair of characteristic wings in the fingerprint plot delineated into C···H/H···C (Figs. 12c and 13*d*). The C···H/H···C interactions are represented by the spikes at the bottom right and left ($d_e + d_i \approx 2.60 - 2.75$Å). The percentage of C···H/H···C increases from compound **12** (6.6%) to **5** (23.9%), in agreement with the substituted group. However, unlike these compounds, no significant C—H···$\pi$ interaction was observed in compounds **8, 14** and **17**.

Noteworthy here also the fact that in the crystals **8, 12, 14** and **17**, a fairly significant contributor 7.8, 5.2, 8.1 and 5.1% respectively has C···C contacts. They are shown on the fingerprint plots as areas on the diagonal at $d_e = d_i \approx$ 1.6-1.7Å (Fig. 12e). These contacts correspond to the presence of the above mentioned $\pi\cdots\pi$ stacking interactions in the crystal structures **8, 12, 14** and **17** (Figs. 12c and 13e). The contribution of C···O/O···C contacts in compounds **8** (4.2%), **11** (4.9%) and **17** (6.1%) (Fig. 13f) was due to the presence of short interatomic C···O (C33—O4 and C16—O10) contacts between *Mol A* and *Mol B*, and was apparent as the pair of tips at $d_e + d_i \approx$ 3.2Å in **8**, while it was due to the presence of short C13—O4 contacts and is apparent as the pair of tips at $d_e + d_i \approx$ 3.1Å in **11** and of short O4—C11contacts as the pairs of tips at $d_e + d_i \approx$ 3.25Å in **17**. The structures are further characterized by a significant proportion of H···X/X···H (H···Br/Br···H in **8, 11** and **12** or H···F/F···H in **14**) contacts, comprising from 9.6% to 19.2% for the molecular surface (Fig. 13g). The pair of spikes in the fingerprint plot delineated into H···F/F···H contacts has tips at $d_e + d_i \approx$ 2.7Å. The pair of characteristic wings in the fringerprint plot delineated into H···Br/Br···H contacts has tips at $d_e + d_i \approx$ 3.05Å (**8**), 3.10 Å (**11**) and 2.9 Å (**12**).The significant contributions from H···X/X···H contacts indicate that the interatomic distances are equal to or greater than the sum of their van der Waals radii, suggesting that they have a limited influence on the molecular packing.

In compound **14**, the structure is further characterized by a significant proportion of F···O contacts, comprising about 8.3% of the molecular surface. The shortest F···O contacts are shown on the fingerprint plots as a pair of spikes at $d_e \approx d_i \approx$ 1.45 Å (Fig. 13h).

The small contributions from the other remaining interatomic contacts have a negligible influence on the packing (Table S2).

### 3.4. Frontier Molecular Orbitals (FMOs)

The HOMO and LUMO energies provided important clues about the chemical behaviors of molecules. All molecular calculations were performed in the gas phase using Density Functional Theory (DFT) with the B3LYP exchange correlation functional. The bond lengthsand bond angles, are listed in Table S1, together with the X-ray parameters. The differences between calculated and experimental bond lengths and angles were within a few Angstroms

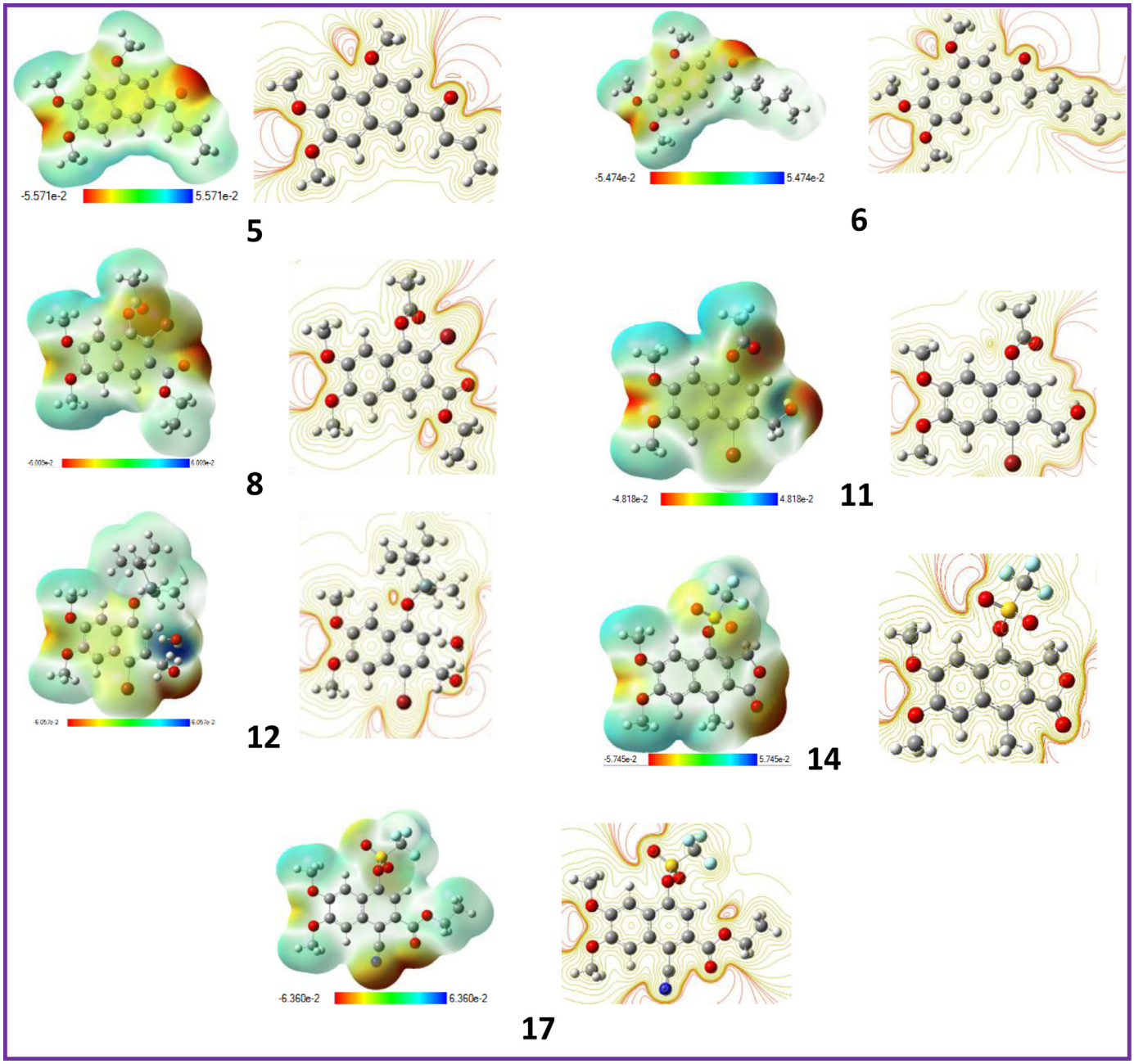


**Fig. 15.** The contour map of electrostatic potential and the total electron density mapped with electrostatic potential of **5, 6, 8, 11, 12, 14** and **17** at an isosurface value of 0.020 a.u. and an isodensity of 0.0004 a.u.

and degrees, respectively, when compared to the experimental parameters which are an isolated molecule in DFT optimization and the crystalline phase in X-ray crystallography analysis. The frontier molecular orbitals of the HOMO and LUMO for all compounds are shown in Fig. 14. The positive and negative phases are shown in red and green, respectively. The energies of HOMO and LUMO, energy gap, electronegativity ($\chi$), chemical hardness ($\eta$), global softness ($\xi$), dipole moment (D) and electrophilicity ($\psi$) index were calculated and are presented in Table 3. The HOMO-LUMO energy gap for **5** is founded to bethelowest, whereas a higher band gap was observed for the other compounds; this indicates that compound **5** exhibits higher chemical reactivity. Furthermore, the chemical potential index for **17** was greater than that of the other compounds, therefore **17** behaves as good electron donor. The dipole moment (D) of compound **14** was greater than that of the othercompounds studied , therefore we can say that these compounds are more reactive than the other compounds. The chemical hardness of **5** was smaller than that of the other compounds, indicating that the electrons are attracted from compound **5**. According to the electrophilicity calculation of all the compounds, we observed that molecule **17** has a larger global electrophilic index compared to the other molecules, as a result, it is more stable than the other compounds. The higher electronegativity value of molecule **17** is indicative of its chemical reactivity.

### 3.5. Molecular Properties

#### 3.5.1. Mulliken population analysis

The Mulliken charge values of the synthesized molecules were calculated using B3LYP functional with 6-311G(d,p) basis set for

all the structures. The calculated Mulliken charge values of the molecules are reported in Table S3. The carbon atom has a positive charge when it is attached to O1, O3, O4, O5 and O6, while the other carbon atom has a negative charges. Moreover, all the hydrogen atoms in the hydroxyl group (**11** and **12**) and attached to water molecule (**12**) have a net positive charge. In all compounds, all oxygen atoms possess negative Mulliken charges, but the charges of O3 are more negative.

*3.5.2. Molecular Electrostatic Potential (MEP)*

In this study, the molecular electrostatic potential of all the compounds was computed using B3LYP/6-311G (d, p) optimized geometry . The contour and surface map is shown in Fig. 15. The negative electrostatic potential is indicated by red regions (nucleophilic reactivity), the blue region indicates the partially positive charge (electrophilic reactivity), the yellow region reveals the slightly rich electron and the green region shows neutral. For all compounds, the total electron density surface mapped with the electrostatic potential indicates the presence of a high negative charge on the O4 atom of the carbonyl oxygen atom (**5, 6, 8, 11** and **14**), while the rest of the compounds have localized oxygen atoms of the hydroxyl (**11** and **12**) and carbonitrile (**17**) groups. Althoughthe positive regions of the MEP map are related to nucleophilic reactivity, these regions cover C-H bonds, hydroxyl group (**11**) and the water molecule (**12)** (Fig. 15). Analyses of the MEP surface of these compounds represent the availability of electrons for possible interaction with another group of atoms. The MEP results are supported by the electrostatic potential contour map showing the isosurface lines in Fig. 15.

## Conclusion

In conclusion, we have developed the synthesis of a novel series of methoxynaphthalene derivatives: **2**-**17** in good yield based on simple and convenient methods. The structure of seven compounds **5, 6, 8, 11, 12, 14** and **17** was identified using single crystal X-ray crystallography and spectroscopic techniques: IR, $^{1}H$, $^{13}C$ NMR and LC/HRMS. Moreover, the methods used provide access to various substituted naphthalene derivatives whose biological activities have not been previously described. X-ray crystallographic studies for **5, 6, 8, 12, 14** and **17** display intermolecular C/O—H···O hydrogen bonding, forming layers in the crystal lattice and stabilized by C—H···$\pi$ or $\pi\cdots\pi$ interactions. The results of HS analysis indicate that the major interactions were found for H···H and O···H/H···O interactions of the total HS area. Further, the structural parameters obtained by DFT calculations substantiate the X-ray crystal structure. The molecular electrostatic potential indicates that the carbonyl oxygen atom is the most negative region. As a result, it is expected that this research will be beneficial for the design, synthesis and various applications of new methoxynaphthalene-based compounds.

## Credit authorship contribution statement

**El-Mahdi Ourhzif**: Synthesis, Performed the experiments, Spectroscopic characterizations, Writing-original draft.

**Isabelle Abrunhosa-Thomas:** Product and material order tracking

**Pierre Chalard:** Visualization, Investigation

**Mostafa Khouili**: Funding acquisition, Project administration,

**Yves Troin:** Supervision, Methodology, Funding acquisition

**Mohamed Akssira**: Conceptualization, Supervision, Writing - review & editing.

**El Mostafa Ketatni**: Methodology, Software, Validation, Writing - review & editing.

## Funding

This work was supported by Campus France (CAMPUS : 36758 VA) and the National Centre for Scientific and Technical Research of Morocco (PHC Toubkal 17/55) (E-M.O.).

## Declaration of Competing Interest

The authors declare that they have no known competing financial interests or personal relationships that could have appeared to influence the work reported in this paper.

## Acknowledgments

The authors are grateful to thank to Dr. Laurent Jouffret (UCA-PARTNER, Institut de Chimie de Clermont-Ferrand, CNRS, Université Clermont Auvergne, SIGMA Clermont, Clermont-Ferrand, France) for the X-ray measurements.

## Supplementary materials

Supplementary material associated with this article can be found, in the online version, at doi:10.1016/j.molstruc.2021.130947.

## References

[1] H. Zhang, Z. Guo, N. Wu, W. Xu, L. Han, N. Li, Y. Han, Two novel naphthalene glucosides and an anthraquinone isolated from rumex dentatus and their antiproliferation Activities in Four Cell Lines, Molecules 17 (2012) 843–850.
[2] S. Onkar, A. Mohammed, A. Nida, New antifungal aromatic compounds from the seeds of rhus coriaria l, Int. Res. J. Pharm. 2 (2011) 188–194.
[3] J. Dai, Y. Liu, Y.-D. Zhou, D.G. Nagle, Cytotoxic metabolites from an indonesian sponge *Lendenfeldia* sp, J. Nat. Prod. 70 (2007) 1824–1826.
[4] J.-C. Lee, C.-H. Lee, C.-L. Su, C.-W. Huang, H.-S. Liu, C.-N. Lin, S.-J. Won, Justicidin A decreases the level of cytosolic Ku70 leading to apoptosis in human colorectal cancer cells, Carcinogenesis 26 (2005) 1716–1730.
[5] M.C. Kozlowski, B.J. Morgan, E.C. Linton, Total synthesis of chiral biaryl natural products by asymmetric biaryl coupling, Chem. Soc. Rev. 38 (2009) 3193–3207.
[6] D. Subramaniam, P. Giridharan, N. Murmu, N.P. Shankaranarayanan, R. May, C.W. Houchem, R.P. Ramanujam, A. Balakrishnan, R.A. Vishwakarma, S. Anant, Activation of apoptosis by 1-hydroxy-5,7-dimethoxy-2-naphthalene-carboxaldehyde, a novel compound from *Aegle marmelos Cancer.Res* 68 (2008) 8573–8581.
[7] N. Abdissa, F. Pan, A. Gruhonjic, J. Grafènstein, P.A. Fitzpatrick, G. Landberg, K. Rissanen, A. Yenesew, M. Erdelyi, Naphthalene derivatives from the roots of *Pentas parvifolia* and *Pentas bussei*, J. Nat. Prod. 79 (2016) 2181–2187.
[8] J.R. Liou, M. El-Shazly, Y.C. Du, C.N. Tseng, T.L. Hwang, Y.L. Chuang, Y.M. Hsu, P.W. Hsieh, C.C. Wu, S.L. Chen, 1,5-Diphenylpent-3-en-1-ynes and methyl naphthalene carboxylates from *Lawsonia inermis* and their anti-inflammatory activity, Phytochemistry 88 (2013) 67–73.
[9] O. Silva, E.T. Gomes, Guieranone A, a naphthyl butenone from the leaves of *Guiera senegalensis* with antifungal activity, J. Nat. Prod. 66 (2003) 447–449.
[10] L.K. Ho, M.J. Don, H.C. Chen, S.F. Yeh, J.M. Chen, Inhibition of hepatitis B surface antigen secretion on human hepatoma cells. components from *Eubia cordifolia*, J. Nat. Prod. 59 (1996) 330–333.
[11] C.C. Chen, W.C. Hsin, F.N. Ko, Y.L. Huang, J.C. Ou, C.M. Teng, Antiplatelet arylnaphthalide lignans from *Justicia procumbens*, J. Nat. Prod. 59 (1996) 1149–1150.
[12] Y. Zhang, K. Wang, H. Chen, R. He, R. Cai, J. Li, D. Zhou, W. Liu, X. Huang, R. Yang, S. Deng, J. Li, X. Guan, Anti-inflammatory lignans and phenylethanoid glycosides from the root of Isodon ternifolius (D.Don) Kudô, Phytochemistry 153 (2018) 36–47.
[13] R.B. Teponno, S. Kusari, M. Spiteller, Recent advances in research on lignans and neolignans, Nat. Prod. Rep. 33 (2016) 1044–1092.
[14] S.R. Flanagan, D.C. Harrowven, M.A. Bradley, A new benzannulation reaction and its application in the multiple parallel synthesis of arylnaphthalene lignans, Tetrahedron 58 (2002) 5989–6001.
[15] B.H. Lipshutz, E. Slack, R. Seupel, D. Aue, G. Bringmann, Atroposelective total synthesis of the fourfold ortho-substituted naphthyltetrahydroisoquinoline biaryl *O,N*-dimethylhamatine, Chem. Eur. J. 25 (2019) 1–10.
[16] J. Youm, H. Lee, Y. Choi, J. Yoon, DW2008S and its major constituents from *Justicia procumbens* exert anti-asthmatic effect via multitargeting activity, J. Cell. Mol. Med. 22 (2018) 2680–2691.
[17] J.L. Woodard, A.C. Huntsman, P.A. Patel, H.-B. Chai, R. Kanagasabai, S. Karmahapatra, A.N. Young, Y. Ren, M.S. Cole, D. Herrera, J.C. Yalowich, A.D. Kinghorn, J.E. Burdette, J.R. Fuchs, Synthesis and antiproliferative activity of derivatives of the phyllanthusmin class of arylnaphthalene lignan lactones, Bioorg. Med. Chem. 26 (2018) 2354–2364.

[18] G. Wang, W. Liu, Z. Gong, Y. Huang, Y. Li, Z. Peng, Synthesis, biological evaluation, and molecular modelling of new naphthalene-chalcone derivatives as potential anticancer agents on MCF-7 breast cancer cells by targeting tubulin colchicine binding site, J. Enzyme. Inhib. Med. Chem. 35 (2020) 139–144.
[19] J. Asano, K. Chiba, M. Tada, T. Yoshil, Antiviral activity of lignans and their glycosides from *Justicia procumbens*, Phytochemistry 42 (1996) 713–717.
[20] T. Ieyama, M.D. Gunawan-Puteri, J. Kawabata, $\alpha$-Glucosidase inhibitors from the bulb of *Eleutherine Americana*, Food. Chem. 128 (2011) 308–311.
[21] M.I. Chung, S.J. Jou, T.H. Cheng, C.N. Lin, F.N. Ko, C.M. Teng, Antiplatelet constituents of formosan Rubia akane, J. Nat. Prod. 57 (1994) 313–316.
[22] H.-J. Zhang, E. Rumschlag-Booms, Y.-F. Guan, D.-Y. Wang, K.-L. Liu, W.-F. Li, V.H. Nguyen, N.M. Cuong, D.D. Soejarto, H.H.S. Fong, L. Rong, Potent inhibitor of drug-resistant HIV-1 strains identified from the medicinal plant *Justicia gendarussa*, J. Nat. Prod. 80 (2017) 1798–1807.
[23] Y.F. Hallock, K.P. Manfredi, J.W. Blunt, J.H. Cardellina, M. Schaeffer, K.P. Gulden, G. Bringmann, Y.A. Lee, J. Clardy, G. Frangois, M.R. Boyd, A-D. Korupensamines, novel antimalarial alkaloids from *Ancistrocladus korupensis*, J. Org. Chem. 59 (1994) 6349–6355.
[24] S. Makar, T. Saha, S.K. Singh, Naphthalene, a versatile platform in medicinal chemistry: Sky-high perspective, Eur. J. Med. Chem. 161 (2019) 252–276.
[25] V. Kuete, T. Eichhorn, B. Wiench, B. Krusche, T. Efferth, Cytotoxicity, anti-angiogenic, apoptotic effects and transcript profiling of a naturally occurring naphthyl butenone, guieranone A, Cell. Divi. 7 (2012) 16.
[26] J .E. Anthony, The larger acenes: versatile organic semiconductors, Angew. Chem. Int. Ed. 47 (2008) 452–483.
[27] M.D. Watson, A. Fechtenkötter, K. Müllen, Big Is beautiful—"aromaticity" revisited from the viewpoint of macromolecular and supramolecular benzene chemistry, Chem. Rev. 101 (2001) 1267–1300.
[28] J.-J. Lee, B.C. Noll, B.D. Smith, Fluorescent chemosensor for chloroalkanes, Org. Lett. 10 (2008) 1735–1738.
[29] J. Svoboda, V. Novotná, V. Kozmik, M. Glogarová, W. Weissflog, S. Diele, A G., Pelzl, novel type of banana liquid crystals based on 1-substituted naphthalene-2,7-diol cores, J. Mater. Chem. 13 (2003) 2104–2110.
[30] R.A. Reddy, U. Baumeister, C. Keith, C. Schierske, Influence of the core structure on the development of polar order and superstructural chirality in liquid crystalline phases ormed by silylated bent-core molecules: naphthalene derivatives, J. Mater. Chem. 17 (2007) 62–75.
[31] C.B. de Koning, A.L. Rousseau, W.A.L. Van Otterlo, Modern methods for the sythesis of substituted naphthalenes, Tetrahedron 59 (2003) 7–36.
[32] C.B. de Koning, J.P. Michael, A.L. Rousseau, A novel method for the synthesis of substituted naphthalenes and phenanthrenes, J. Chem. Soc, Perkin Trans. 1 (2000) 787–797.
[33] J.-G. Wang, M. Wang, J.-C. Xiang, Y.-P. Zhu, W.-J. Xue, W.A.-X. Wu, Direct Synthesis of Substituted Naphthalenes from 1,3-Dicarbonyl Compounds and 1,2 Bis(halomethyl)benzenes Including a Novel Rearrangement Aromatization of Benzo[c]oxepine, Org. Lett. 14 (2012) 6060–6063.
[34] C.K. Bradsher, Formation of six-membered aromatic rings by cyclialkylation of some aldehydes and ketones, Chem. Rev. 87 (1987) 1277–1297.
[35] W.S. Johnson, G.H. Daub, The Stobbe condensation in Organic Reactions, Wiley New York. 6 (1951) 1–73.
[36] E.M. Mmutlane, J.P. Michael, I.R. Green, C.B. De Koning, The synthesis of ventiloquinone L, the monomer of cardinalin 3, Org. Biomol. Chem 2 (2004) 2461–2470.
[37] C.B. de Koning, S.S. Manzini, J.P. Michael, E.M. Mmutlane, T.R. Tshabidi, W.A.L. Van Otterlo, Base- and light-assisted synthesis of anthracenes from 3-allylnaphthalene-2-carbaldehydes, Tetrahedron 61 (2005) 555–564.
[38] E-M. Ourhzif, A. Pâris, I. Abrunhosa- Thomas, El M. Ketatni, P. Chalard, M. Khouili, R. Daniellou, Y. Troin, M. Akssira, Design, synthesis and evaluation of cytotoxic activities of arylnaphthalene lignans and aza-analogs, Arch Pharm (2021) e2000479.
[39] E.M. Ourhzif, C. Decombat, I. Abrunhosa-Thomas, L. Delort, M. Khouili, M. Akssira, F. Caldefie-Chezet, P. Chalard, Y. Troin, Synthesis and biological evaluation of new naphthoquinones derivatives, Curr. Org. Synth. 17 (2020) 224–229.
[40] Bruker*APEX3* (Version 5.054), SAINT+ (Version 6.36A), *SADABS*, Bruker AXS Inc., Madison, Wisconsin, USA, 2016.
[41] G.M. Sheldrick, Acta Crystallogr. Sect. A Found, Crystallogr. 71 (2015) 3–8.
[42] G.M. Sheldrick, Acta Crystallogr. Sect. C Struct, Chem. 71 (2015) 3–8.
[43] K. Brandenburg, DIAMOND, Crystal Impact GbR, B Bonn, Germany, 2006.
[44] M.A. Spackman, D. Jayatilaka, CrystEngComm. 11 (2009) 19–32.
[45] J.J. McKinnon, D. Jayatilaka, M.A. Spackman, Chem. Commun. (2007) 3814–3816.
[46] M.J. Turner, J.J. MacKinnon, S.K. Wolff, D.J. Grimwood, P.R. Spackman, D. Jayatilaka, M.A. Spackman, Crystal Explorer 17.5, University of Western Australia, Perth, Australia, 2017.
[47] M. Frisch, G. Trucks, H. Schlegel, G. Scuseria, Gaussian 09, revision D. 01, 2009.
[48] A. Frisch, A. Nielson, A.J. Holder, Gaussview user manual, 556, Gaussian Inc, Pittsburgh, PA, 2000.
[49] A.D. Becke, J. Chem. Phys. 98 (1993) 5648–5652.
[50] C. Lee, W. Yang, R.G. Parr, Phys. Rev B. 37 (1988) 785–789.
[51] G. Miehlich, A. Savin, A. Stoll, H. Preuss, Chemical Physics Letters 157 (1989) 200–206.
[52] S. Nahm, S.M. Weinreb, N-methoxy-N-methylamides as effective acylating agents, Tetrahedron Lett 22 (1981) 3815–3818.
[53] M.P. Sibi, Chemistry of N-methoxy-N-methylamides. Applications in synthesis. A review, Org. Prep. Proced. Int. 25 (1993) 15–40.
[54] M. Mentzel, H.M.R. Hoffmann, N-methoxy-N-methylamides (Weinreb amides) in modern organic synthesis, J. Prakt. Chem /Chem-Ztg. 339 (1997) 517–524.
[55] V. Trommer, F. Fischer, M. Hapke, Novel naphthylpyridines from cobalt–catalyzed cyclotrimerization of a chiral diyne, Monatsh Chem 149 (2018) 755–763.
[56] M. Yoshizawa, T. Itoh, T. Hori, A. Kato, Y. Anami, N. Yoshimoto, K. Yamamoto, Identification of the histidine residue in vitamin D receptor that covalently binds to electrophilic ligands, J. Med. Chem. 61 (2018) 6339–6349.
[57] D.L. Boger, P. Turnbull, Synthesis and Evaluation of a carbocyclic analogue of the CC-1065 and duocarmycin alkylation subunits: Role of the vinylogous amide and implications on DNA alkylation catalysis, J. Org. Chem. 63 (1998) 8004–8011.
[58] E.D. Slack, R. Seupel, D.H. Aue, G. Bringmann, B.H. Lipshutz, atroposelective total synthesis of the fourfold ortho-substituted naphthyltetrahydroisoquinoline biaryl O,N-dimethylhamatine, Chem. Eur. J. 25 (2019) 14237–14245.
[59] J.P. Deville, V. Behar, Tandem conjugate cyanide addition-Dieckmann condensation in the synthesis of the ABCD-ring system of Lactonamycin, Org. Lett. 4 (2002) 1403–1405.
[60] Q. Zhang, J. Dong, J. Cui, G. Huang, Q. Meng, S. Li, Cytotoxicity of synthesized 1,4-naphthoquinone oxime derivatives on selected human cancer cell lines, Chem. Pharm. Bull (66) (2018) 612–619.
[61] M.J. James, J.L. Schwartz, F. Strieth-Kalthoff, B. Wibbeling, F.J. Glorius, Am. Chem. Soc. 140 (2018) 8624–8628.
[62] E.R. Zubarev, S.I. Stupp, Dendron Rodcoils: Synthesis of novel organic hybrid structures, J. Am. Chem. Soc. 124 (2002) 5762–5773.
[63] N. Vila, P. Besada, D. Vina, M. Sturlese, S. Moro, C. Teran, Synthesis, biological evaluation and molecular modeling studies of phthalazin-1(2H)-one derivatives as novel cholinesterase inhibitors, RSC Adv 6 (2016) 46170–46185.
[64] J. Roger, J-C. Hierso, Phenol derivatives in ruthenium-catalyzed C–H arylation: A general synthetic access to azole-based congested polyaromatics, Eur. J. Org. Chem. (2018) 4953–4958.
[65] D. Wang, L. Kuang, Li Z, K. Ding, *L*-Proline-Promoted Rosenmund-von Braun Reaction, Synlett (1) (2008) 69–72.